3D directional tuning in the orofacial sensorimotor cortex during natural feeding and drinking

Victoria B. Hosack[1] and Fritzie I. Arce-McShane[1,2,3]

[1]Department of Oral Health Sciences, School of Dentistry, University of Washington, Seattle, WA
[2]Division of Neuroscience, Washington National Primate Research Center, University of Washington, Seattle, WA
[3]Graduate Program in Neuroscience, University of Washington, Seattle, WA

Abstract

Directional tongue movements are crucial for feeding and speech, ensuring proper food positioning for chewing and swallowing, as well as accurate sound production. While directional tuning in the arm region of the sensorimotor cortex during reaching tasks is well-studied, little is known about how 3D tongue direction is encoded in the orofacial sensorimotor cortex (OSMCx) during natural behaviors. Understanding this neural representation has important implications for rehabilitating individuals with orolingual dysfunctions. This study examines the directional tuning and population dynamics in OSMCx during naturalistic feeding and drinking, and how these are affected by sensory loss. Using biplanar videoradiography, we tracked implanted tongue markers in behaving rhesus macaques (*Macaca mulatta*) and simultaneously recorded 3D positional data with spiking activity from chronically implanted microelectrode arrays in primary motor (MIo) and somatosensory (SIo) areas of the orofacial cortex. In some sessions, tasks were preceded by bilateral nerve block injections to the sensory branches of the trigeminal nerve. Modulation to 3D tongue direction during feeding and drinking was found in most MIo and SIo neurons. Directional information in both individual- and population-level was higher in feeding and was more robust in MIo. Following sensory loss, alterations in tongue kinematics were accompanied by changes in directional information in MIo and SIo, manifesting as modifications in both individual neuron tuning characteristics and the broader dynamics of population-level neural activity. Overall, this study advances our understanding of how OSMCx contributes to complex, coordinated control of naturalistic tongue movements. It expands our current knowledge of orofacial control to three dimensions and demonstrates the specificity and adaptability of population activity in MIo and SIo in response to different behavioral contexts.

Introduction

Motor and somatosensory cortical neurons modulate their spiking activity based on movement direction as seen in arm reaching tasks (Georgopoulos et al., 1988; Schwartz et al., 1988a; Prud'homme and Kalaska, 1994) and orofacial behaviors. In the primary motor (MIo) and primary somatosensory (SIo) areas of the orofacial sensorimotor cortex (OSMCx), neurons encode the direction of voluntary tongue protrusion (Murray and Sessle, 1992; Lin et al., 1994a) and semi-automatic tongue movements in chewing and swallowing (Sessle et al., 2005b). Extensive research has explored how the arm region of the sensorimotor cortex encodes movement direction (Ajemian et al., 2000; Georgopoulos et al., 2007; Churchland et al., 2012; Lillicrap and Scott, 2013). Since the tongue is enclosed within the oral cavity and thus hidden from view, it has proved difficult to study the neuromechanical processes underlying directional tongue movements that are essential for these behaviors (Hiiemae and Palmer, 2003). Thus, considerably less is known about how 3D tongue direction is encoded in the OSMCx and the role of tactile sensation (Bach-y-Rita et al., 1998; Lamm et al., 2005; Lozano et al., 2009) during natural feeding and drinking. This knowledge has important implications for improving evaluation and treatment strategies for individuals with sensorimotor dysfunctions (Takizawa et al., 2016; Avivi-Arber and Sessle, 2017).

The OSMCx plays an important role in the coordination of complex tongue movements. Seminal studies on the directional tuning properties of OSMCx neurons by Sessle and colleagues employed varying locations of spouts that delivered a juice reward to elicit directional tongue protrusions without tracking tongue movements. A later study incorporated tracking of 2D tongue movements using videofluoroscopy during voluntary directional protrusions (Arce et al., 2013), but the tongue trajectories were not used to study directional tuning. In all these prior studies, primates have been trained to interact with a computer display to elicit a tongue protrusion to a specific direction on cue. There is a knowledge gap on how spiking activity in the OSMCx relates to tongue movements during natural behaviors. With the development of biplanar video-radiography (Brainerd et al., 2010), it is now possible to track these 3D tongue movements within the oral cavity at a high temporal and spatial resolution (Montuelle et al., 2020; Feilich et al., 2021). By simultaneous recording of precise tongue movements and spiking activity, we have shown recently that tongue position and shape can be accurately decoded from OSMCx during feeding (Laurence-Chasen et al., 2023).

Our study investigated how OSMCx encodes and decodes tongue direction during untrained feeding and drinking, comparing activity across multiple cortical regions. Given the importance of oral somatosensation in tongue positioning and bolus control during chewing and swallowing (Smith and Cutrer, 2011), we also examined its role in sensorimotor control by selectively blocking oral tactile sensation.

Methods

Subjects. Experiments were performed on two adult male rhesus macaques (*Macaca mulatta,* 9–10 kg, ages 8 and 9 years) in the University of Chicago XROMM Facility. This sample size was chosen based on precedent in the field of non-human primate motor neuroscience. All protocols were approved by the University of Chicago Animal Care and Use Committee and complied with the National Institutes of Health Guide for the Care and Use of Laboratory Animals.

The subjects were seated in a standard primate chair and head-fixed to keep their head position constant during feeding and drinking trials. Each trial lasted 10 seconds. In a feeding trial, a piece of food (grape, gummy bear, pasta) of roughly the same size was presented directly to the animals' mouth using a stylus. In a drinking trial, juice was delivered through one of three spouts positioned in front of the subject (Fig. 1A).

Cranial Nerve V anesthesia. For some sessions, these behavioral tasks were preceded by nerve block injections (0.25% Bupivacaine HCL and Epinephrine 1:200,000, 0.25 mL/injection site) to the sensory branches of bilateral trigeminal nerves (lingual, inferior alveolar, buccal, palatine) to eliminate oral tactile sensation locally and temporarily. The nerve block was administered while the subjects were under sedation, and all data were collected within 90 minutes of the nerve block. Each monkey served as its own control, with nerve block feeding data collection sessions taking place either a day before or a day after the associated control session. Nerve block drinking data collection was performed immediately following the control drinking session. Multiple datasets (40-60 trials) were collected for both subjects across multiple days. However, due to the complex and time-consuming nature of processing integrated XROMM and neural data, one session per subject, behavior, and condition was used for this study. Thus, we analyzed a total of 8 datasets.

Video-radiography. Prior to data collection, the animals were implanted with spherical tantalum beads (1-mm diameter) in the cranium, mandible, and the tongue, from the tip to the region of the circumvallate papillae. During feeding or drinking, the movement of these markers was recorded using high-resolution (200 Hz, <0.1 mm) biplanar video-radiography collected with Xcitex ProCapture version 1.0.3.6. The 3D positional data was obtained following the previously described X-ray Reconstruction of Moving Morphology (XROMM) workflow (Laurence-Chasen et al., 2020) incorporating the use of XMALab (Knörlein et al., 2016) and machine learning using DeepLabCut (Mathis et al., 2018) to reconstruct the kinematic data. The x, y, z values of the markers were then smoothed with a 30 Hz low-pass Butterworth filter and transformed into a cranial coordinate space with the origin fixed at the posterior nasal spine. Gape cycles within each feeding sequence were manually identified and categorized by cycle type (manipulation, stage 1 transport, chew, stage 2 transport, or swallow).

Electrophysiology. Under general anesthesia, a microelectrode array was chronically implanted in four areas of the left hemisphere (Supplementary file 1, Fig. 1): rostral MIo (96-electrode Utah

array; electrode length: 1.5 mm), caudal MIo (32-electrode Floating microelectrode array (FMA), electrode length: 3.0–4.5 mm), area 1/2 (96-electrode Utah array, electrode length: 1.0 mm), and area 3a/3b (32-electrode FMA, electrode length: 4.0–8.7 mm). The neural data was recorded using Grapevine Neural Interface Processor (Ripple Neuro, Salt Lake City, UT). Signals were amplified and bandpass filtered between 0.1 Hz and 7.5 kHz and recorded digitally (16-bit) at 30 kHz per channel. Only waveforms (1.7 ms in duration; 48 sample time points per waveform) that crossed a threshold were stored and offline spike sorted (Offline Sorter, Plexon, Dallas, TX) to remove noise and to isolate individual neurons. Neurons recorded during control feeding sessions are the same as those previously reported on in Laurence-Chasen et al., 2023. The channel name assigned to each recorded neuron was kept consistent between control and nerve block data for comparison.

Data analysis

***3D kinematics*.** 3D tongue kinematics were recorded simultaneously with the neural data in all behavioral sessions. All data analyses were performed in MATLAB 2022b (MathWorks, Natick, MA). For feeding, the instantaneous 3D direction of the tongue tip marker for every 100 ms throughout each gape cycle was calculated as:

3D angle, $\theta = \tan^{-1}(\|v_1 \times v_2\| / v_1 \cdot v_2)$ (1)

Where v_1 is the x, y, z position at the start of each 100-ms interval and v_2 is the position at the end (Fig. 1B). These directions were then categorized based on whether the movement was negative or positive relative to the horizontal plane (Left/Right), the sagittal plane (Inferior/Superior), and the x axis (Posterior/Anterior). This resulted in eight directions: AntSupL, AntSupR, AntInfL, AntInfR, PostSupL, PostSupR, PostInfL, and PostInfR. An equal number of 100-ms intervals from each of these directions was sampled to eliminate the possible effect of different distributions of kinematics across datasets, and spike data during each interval was used for neural analysis. For comparison with the drinking task, the sign was determined relative to the horizontal plane, with rightward tongue movement being positive. This is also the plane of motion which has been the least studied. These left-right directions were categorized into six 10°-bins with a total range of -30° to 30°, which encapsulated most of the observed distribution of directions in each subject. Lingual yaw (transverse rotation) and pitch (elevation/depression) were also calculated to compare tuning across the lateral and vertical components of tongue direction (Supplementary file 2, Equation 2). For drinking, the direction was determined by which of the three spouts juice was dispensed from during each lick. The spiking activity used for neural analysis of the drinking task was from intervals of ±250 ms around each minimum protrusion of the tongue. As 100 ms was not sufficient to capture the full range of tongue motion during each drinking cycle, the length of time used was increased to allow a clear distinction between the three directions. The period of 250 ms spans about 75% of the average lick length from minimum to maximum protrusion of the tongue.

Kinematic performance for feeding was determined by the spread of tongue directions observed across trials. For drinking trials, performance was determined by the variance of endpoint positions as well as by the proportion of "failed" cycles, where the monkey missed the correct spout location with their tongue tip. The difference between control and nerve block performance was evaluated using a two-tailed t-test and f-test.

Directional tuning of single neurons. Tongue directions were subsequently compared with the firing rates of individual neurons across cortical areas. To determine if neurons were directionally modulated, we used a bootstrap procedure (Arce et al., 2010): we resampled the firing rates from an equal number of trials in each direction with replacement 1000 times and computed 95% confidence intervals from the resulting distribution to test whether the mean ranks are the same across directions. The proportions of neurons that were found to be directionally tuned were compared across groups using a chi-square test. Due to limited neuron counts in some cortical regions, we combined rM1 and cM1 recordings as MIo, and areas 1/2 and 3a/3b as SIo for subsequent analyses (Supplementary file 1, Table 1). Then, multiple linear regression was used to determine if the firing of each neuron fit the cosine tuning function that has been previously described for the arm area of the motor cortex (Schwartz et al., 1988b). To accomplish this, the directional components of a unit vector representing each group of directions were calculated. For neurons that fit the tuning function, a preferred direction (PD) in 3D space was estimated. These PDs are distributed around a unit sphere, with the origin representing the start of the movement. The directional index was calculated as a measure of the depth of directional tuning. To determine PDs for the drinking task, we resampled the original distribution of firing rates with replacement for each direction and calculated the direction for which a neuron exhibited its maximal firing rate over 1000 bootstrap samples. Similarly, a PD across the left-right feeding directions was determined for comparison. Circular concentration (k-test) to compare distributions of PDs during feeding and polar plot generation were performed using the CircStat MATLAB toolbox (Berens, 2009). For drinking, distributions of PDs were compared using a chi-square test. We analyzed the trial-by-trial variability of neuronal activity using the Fano factor, which was computed as the spike-count variance divided by spike-count mean within each session. The Fano Factor was calculated separately for each subject, task, and cortical region. For analysis across sessions, we used the mean-matched Fano factor (Churchland et al., 2010).

Factor Analysis of population activity. We used Factor Analysis (FA), a linear dimensionality reduction method, to obtain latent trajectories of spiking activity and compare population responses to different directions across trials. FA defined as:

$y \sim N(\mu, CC' + R)$ (2)

where y is the spike counts from n neurons, $\boldsymbol{\mu}$ is the mean spike counts from **n** neurons, $\boldsymbol{C}$ (m × n) is the loading matrix mapping **m** latent factors to the spike counts of **n** neurons, and $\boldsymbol{R}$ (n × n)

represents the unexplained variance of independent neurons(Santhanam et al., 2009; Horrocks et al., 2024). The parameters $\boldsymbol{\mu}$, $\boldsymbol{C}$ and $\boldsymbol{R}$ were estimated with expectation-maximization using DataHigh Matlab toolbox (Cowley et al., 2013). The latent factor space obtained using FA represents the shared population variance of neurons. To obtain latent factors of shared population activity, we binned the spike times of each neuron into 10 ms bins (10 bins for feeding; 50 bins for drinking). Neurons with a mean firing rate < 1.0 spike/s were excluded and the resultant vectors were smoothed using a Gaussian kernel with a 10 ms standard deviation (SD). To determine the dimensionality of the latent variable, we used 3-fold cross-validation to find the value of **m** which maximized the likelihood of the data. We then obtained an FA model by fitting an m-dimensional latent factor model. FA was performed using trial-averaged data to examine the direction-relevant latent factor responses (i.e., neural population trajectories).

We quantified directional differences in population activity by calculating the Euclidean distance over **m** latent factors) between trial-averaged neural population trajectories for each unique direction pair (drinking = 3 pairs; feeding = 28 pairs). This analysis was performed for every 10 ms bin throughout each trial. To assess differences between experimental conditions (control vs. nerve block) or cortical region (MIo vs. SIo), we applied two-sample t-test to the mean inter-trajectory distances across all direction pairs. We further characterized the neural space spanned by population activity by measuring the cumulative Euclidean distance travelled by trajectories from start to end of a trial.

To control for potential sampling biases, we implemented two critical validation procedures. First, we addressed the varying trial counts across directions in the feeding task by performing Factor Analysis with standardized samples (N = 80 trials per direction) through random subsampling repeated 10 times. We then compared the cumulative explained variance between the full and subsampled datasets. Second, we controlled for population size differences by subsampling MIo and SIo neurons to equivalent counts, enabling unbiased comparison of Factor Analysis results between cortical regions.

To compare behaviors, we performed FA on only caudal MIo neurons that remained stable across both feeding and drinking recording sessions (N = 20). These neurons were determined through a stability test (Dickey et al., 2009), which compared the average waveform and interspike interval for both datasets. We analyzed two subsets of kinematic data: data collected within 200 ms surrounding minimum gape, and data from trials where the 3D angle measured 100 ms after minimum tongue protrusion was between -5 and +5 degrees.

Decoding tongue direction. The ability to predict tongue direction from spiking activity of MIo and SIo neurons was evaluated using a K-nearest neighbor (KNN) classifier. The Euclidean distance was used to identify nearest neighbors, and the number of nearest neighbors used was K = 7. This K value was determined after testing different Ks which yielded comparable results. The feature

was the firing rate of each neuron over each trial: every 100 ms throughout feeding sequence, or 100 ms centered at minimum tongue protrusion during drinking. As a more direct comparison to the drinking, feeding directions were split into three groups representing left, middle, and right movement directions. The decoder was trained on 80% of trials and tested on the remaining 20%, then decoder performance was determined by the percentage of test trials where the direction of movement was correctly decoded from the neural data. We ran 100 iterations of the classifier using a different set of randomly selected training and test trials then calculated the average performance. The same sets of training and test trials were used for decoding from simultaneously recorded MIo and SIo data. However, our recorded populations were of variable sizes, and decoding performance was found to be related to the number of neurons in the ensemble. Because the smallest population of neurons we recorded was 28, we selected 28 random neurons from the larger populations for each iteration. Based on the positive relationship between population size and decoding accuracy, we expect that performance would increase with more neurons. These results will show whether tongue direction can be decoded from a very small number of neurons. We fit a linear regression model with interactions to compare decoding performance across the other variables in the experiment. To determine if a mixed population of MIo and SIo neurons performs better than the pure populations, we started with the full MIo population and systematically replaced 25 MIo neurons with an equal number of SIo neurons. We repeated this replacement over 100 iterations, each with a different random selection of neurons, and decoded tongue direction using the KNN classifier. We compared the average decoding performance of these slightly different mixed populations to the baseline of running the decoder with the full MIo population.

We also decoded tongue direction using a long short-term memory (LSTM) network (Hochreiter and Schmidhuber, 1997; Glaser et al., 2020; Laurence-Chasen et al., 2023; Hahn and Arce-McShane, 2024) implemented in MATLAB's Deep Learning Toolbox. For the feeding task, we analyzed 3D tongue movement direction (relative to the sagittal plane) at 100 ms intervals. For the drinking task, we categorized tongue direction every 500 ms as either left (-45°), middle (0°), or right (45°). For each neural population, we created a 2D array containing spike counts for these time intervals (neurons × intervals). We randomly selected five groups of 28 neurons with replacement from each population. Using 5-fold cross-validation, we trained an LSTM network (400 hidden units, 50 training epochs) on 85% of the intervals. The network was then tested on the remaining 15% of neural data in a stepwise manner, producing a sequence of predicted tongue directions. We used mean R^2 to measure prediction accuracy.

Results

Previous research has investigated directional tuning of OSMCx neurons during trained tongue-protrusion tasks. Our study extends this work by investigating two natural, untrained behaviors: feeding and licking ("drinking") from a spout. These behaviors provide distinct contexts for

studying tongue coordination - feeding allows unrestricted tongue movement, while drinking constrains movement direction based on spout location. This comparison enables us to examine how OSMCx coordinates tongue movements under different behavioral contexts.

Neuronal modulation patterns differ between MIo and SIo. Many neurons exhibited significant modulation of spiking activity to tongue direction (bootstrap, $p < 0.05$), though there were diverse patterns. Figure 2 shows peri-event time histograms (PETHs) of two example neurons related to tongue movements during feeding and drinking. In feeding, both neurons showed complex oscillatory firing, with notable peaks between -0.05s to 0.1s for upward movements to the right (MIo, Fig. 2A-left) and posterior movements to the left (SIo, Fig. 2A-right). For drinking there was clear separation between different directions in the MIo neuron, with the left (green) exhibiting the highest activity (Fig. 2B-left), while SIo showed oscillatory patterns with less distinct separation between spout locations, but higher overall activity (Fig. 2B-right). Like the arm region, the tuning curves of directionally modulated MIo and SIo neurons fit the cosine tuning function (*F*-test, $p < 0.05$, feeding: MIo = 86%, SIo = 75%). Figure 3A maps a neuron's firing rate for tongue movements in left-right, inferior-superior, and posterior-anterior axes. Here, a MIo neuron is strongly tuned to posterior-anterior and inferior-superior directions, while remaining unresponsive to left-right movements during natural feeding. Many of the recorded neurons in each population behaved in a similar fashion, with peaks most frequently observed toward the anterior and superior directions. This observation was consistent with the tongue movements being most frequent in the Anterior Superior directions, followed by the Posterior Inferior (Figure 3 – figure supplement 1. The varying neuronal responses to tongue direction could not be attributed to variability in their firing, as the distribution of the Fano factor was similar across directions (Kruskal-Wallis, $p > 0.1$ for all except SIo control drinking $p = 0.06$).

The proportion of directionally tuned neurons was higher in the feeding vs. drinking task (Chi-square, $p < 0.05$, feeding: 72%, drinking: 66%) and differed significantly between MIo and SIo during the feeding task in both subjects (Chi-square, $p < 0.001$). In rostral and caudal MIo, 80% of neurons were modulated to 3D direction (bootstrap, $p < 0.05$, Fig. 3B, left), compared to 52% in areas 1/2 and 3a/3b. Notably, fewer MIo neurons showed directional tuning during swallows compared to chewing, while SIo neurons maintained consistent proportions (Figure 3 – figure supplement 2; Chi-square, MIo: $p < 0.05$, SIo: $p > 0.1$). During drinking, the proportion of directionally modulated neurons was more similar between regions (69% in MIo vs. 60% in SIo: Chi-square, $p > 0.05$, Fig. 3B right). Mean-matched Fano factor was significantly lower in MIo than SIo in both tasks (Wilcoxon rank sum test, $p < 0.001$). We considered that the difference in the directional tuning between the two behaviors could be due to the different time intervals used for each task since the period around minimum tongue protrusion in the drinking may contain more of the sensory inputs from the previous lick. However, when sampling spiking activity from an earlier period in feeding, the percentage of directionally tuned SIo neurons was still

significantly lower than MIo (Chi-square, $p < 0.001$, data not shown). Shifting the period of the drinking trials to be after minimum protrusion also did not lead to a significant difference between MIo and SIo ($p > 0.1$).

Further analysis of the tongue's lateral (yaw) and vertical (pitch) components during feeding revealed additional insights. Figure 4A shows peak activity of a neuron in MIo and in SIo at varying degrees of pitch and yaw. Overall, more neurons responded to pitch than yaw (Fig. 4B), with MIo showing a higher proportion of neurons tuned to both components compared to SIo (Chi-square, yaw: $p < 0.08$, pitch: $p < 0.001$), consistent with our 3D direction results. MIo neurons exhibited sharper and narrower tuning curves than the broader tuning curves observed in SIo (Fig. 4A, see Supplementary file 2).

<u>The peak of the PD distribution coincides with leftward tongue movements.</u> The distribution of preferred directions provides insight into how tongue muscles are coordinated during movement. Intrinsic and extrinsic tongue muscles are involved in shaping the tongue (e.g., elongation, broadening) and positioning the tongue (e.g., protrusion/retraction, elevation/depression), respectively. These muscles receive bilateral motor innervation except for genioglossus. Straight tongue protrusion requires the balanced action of the right and left genioglossi while the lateral protrusion involves primarily the contralateral genioglossus. Given this unilateral innervation pattern, we hypothesized that left MIo/SIo neurons would preferentially respond to leftward tongue movements, corresponding to right genioglossus activation.

During feeding, MIo and SIo showed non-uniform distribution of preferred directions across a unit sphere (Fig. 5; Rayleigh test, $p < 0.001$) and similar directional indices (t-test, $p > 0.1$, mean ± 1 SD: MIo: 0.533 ± 0.3, SIo: 0.604 ± 0.5). As hypothesized, most neuronal populations showed peaks in PD distributions toward leftward tongue movements, except in Monkey R's SIo (Fig. 6A). Similar results were found with the distributions of preferred yaw during feeding (Supplementary file 2, Fig. 4). While feeding showed comparable PD distributions between MIo and SIo in both subjects (circular k-test, $p > 0.1$), drinking revealed significant differences between regions in Monkey R (Chi-square, $p < 0.001$) but not Monkey Y ($p > 0.09$). Monkey Y maintained predominantly left-directed PDs across both tasks, while Monkey R showed more balanced left-right PDs during drinking, suggesting potential involvement of additional muscles beyond the right genioglossus.

<u>Neural population trajectories differed based on task and cortical regions.</u> We analyzed directional tuning at the population level using Factor Analysis (FA) on simultaneously recorded neurons to extract neural trajectories and identify patterns in their shared activity. In both tasks, neural trajectories of population activity in both MIo and SIo exhibited robust directional information; inter-trajectory distances of all unique direction pairs were significantly higher than zero (Fig. 7, t-test, $p < 0.001$, for all comparisons in both subjects and region). Notably in the feeding task, MIo and SIo showed smaller inter-trajectory distances between Anterior-Posterior

paired trajectories during feeding (e.g., AntSupL-brown and PostSupL-green) compared to a greater separation between other directional pairs (Fig. 7-top, t-test, $p < 0.05$ for both monkeys). Paired Superior-Inferior directions, e.g., PostSupL-green and PostInfL-cyan, showed the largest separation, though this difference was not significant ($p > 0.1$). Cumulative explained variance for the first three factors was higher in feeding (MIo: 82%, SIo: 81%) than in drinking (MIo: 74%, SIo: 63%) when all neurons were used for the factor analysis (Fig. 7). Similar results were obtained when equal number of neurons were used (Fig. 7- figure supplement 1). To control for factors such as different neurons and kinematics that might influence the results, we performed factor analysis on stable neurons across both tasks using all trials (Fig. 7- figure supplement 2A) and using trials with similar kinematics (Fig. 7- figure supplement 2B). While the general shape of the population trajectory was preserved across tasks, the inter-trajectory distance between them was significant (t-test, $p < 0.001$, mean ± 1 SD: 0.6786 ± 0.0424). Moreover, the MIo trajectory length was longer in feeding (feeding: 0.8954, drinking: 0.6038) despite similar firing rates across tasks (t-test, $p > 0.05$) and longer tongue displacement in drinking ($p < 0.001$, mean ± 1 SD: feeding: 27.5 ± 9.8, drinking: 47.6 ± 11). When trials were limited to those with similar directional angles (±5 degrees), the difference in trajectory length was no longer observed but the inter-trajectory distance between tasks remained significantly different (t-test, $p < 0.001$, mean ± 1 SD: 0.6967 ± 0.0793).

MIo population trajectories followed a circular path and exhibited consistent patterns based on directional components. For example (Fig. 7 top), trajectories with upward (Sup) components (AntSupL/R, PostSupL/R) rotated opposite from trajectories with downward (Inf) components (AntInfL/R, PostInfL/R). In feeding, Factors 1 and 2 captured superior-inferior and right-left directions, respectively. In drinking, MIo trajectories exhibited consistent rotational direction regardless of spout location (Fig. 7 bottom left), while exhibiting distinct separation of trajectories for left, center, and right spout-directed tongue movements clustering at approximately -0.5, 0, and 0.5 positions along the Factor 2 axis, respectively. Indeed, inter-trajectory distances in Factor 1 were significantly higher in feeding (t-test, $p < 0.001$, mean ± 1 SD: 0.4628 ± 0.0246) than in drinking (mean ± 1 SD: 0.1286 ± 0.0610), indicating that Factor 1 resembled directional information in feeding but a condition-independent feature of population activity in drinking. The latent factors revealed a clear organizational principle: Factor 1 predominantly captured superior-inferior directional components in feeding, while Factor 2 primarily represented left-right directional components of tongue movement in both tasks.

Similar to previous findings (Russo et al., 2018), SIo trajectories in both feeding and drinking showed stark differences from MIo as they were more tangled and exhibited less direct (i.e., sharp turns) paths (Fig. 7 right). Unlike MIo trajectories, SIo trajectories spanned a smaller neural space, had variable distances between trajectories, and showed inconsistent patterns based on directional components. Quantitative analysis revealed greater separation between trial-averaged population trajectories in MIo compared to SIo (Fig. 7 inset, t-test, $p < 0.01$, mean ± 1 SD: MIo: 0.34 ± 0.03; SIo: 0.12 ± 0.02). These results were consistent with significantly longer distance travelled by MIo population trajectories compared to SIo in both tasks for Monkey R only

(t-test, $p < 0.001$, mean ± 1 SD: feeding: MIo: 0.43 ± 0.07; SIo: 0.26 ± 0.09; drinking: MIo: 2.85 ± 0.42; SIo: 1.36 ± 0.52). The regional differences cannot be attributed to fewer SIo neurons used (Figure 7 – figure supplement 3).

Effects of nerve block

Sensation plays a key role in tongue positioning and movements for natural behaviors. During ingestion, tactile feedback is necessary for locating the bolus, preventing tongue bites, feeling where the drinking spout is, and identifying when it is safe to swallow. To evaluate the role of oral sensation, we used a bilateral oral nerve block to temporarily eliminate tactile sensation in the oral cavity and observe how the control of tongue movement was impacted. Below, we show how the loss of sensation affected both tongue kinematics and directional tuning of neurons during feeding and drinking. To verify that differences between the control and nerve block conditions were due to the loss of sensory feedback and not because of other factors such as sedation and injection, a sham experiment was conducted where saline was administered to the injection sites instead of nerve block. No significant changes to tongue kinematics were observed following the sham experiments (Fig. 8).

Changes to tongue kinematics. In feeding, the mean and overall spread of directions were significantly different between the control and nerve block conditions (t-test, $p < 0.01$ and f-test, $p < 0.001$). There was a shift towards a smaller range of 3D directions in Monkey R, whereas there was a shift towards a broader distribution in Monkey Y under the nerve block condition (Fig. 8A). The positions of maximum protrusion of the tongue during drinking, i.e., the endpoints, were also affected by the loss of sensation. These endpoints represent the planned target position of the tongue to receive the juice reward from a specific spout. In the control drinking task, the endpoints for each spout location were very distinct. In contrast, the endpoints of tongue movements in nerve block exhibited a greater overlap across locations and more variance in all three axes of motion, i.e., Posterior-Anterior, Inferior-Superior, and Left-Right (Fig. 8B).

Compared to the control, the trajectories of the tongue tip in the nerve block condition during drinking had a smaller range of Left-Right values. Visually, the tongue trajectories toward the different spout locations were messier and less distinct in failed cycles where the tongue tip missed the location of the correct spout by more than ±2 SD from the mean (Fig. 9). In both monkeys there was a significant increase in the average distance from the mean endpoint position, though this difference was much greater in Monkey R (Fig. 8C). We noted a difference between subjects in the frequency of failed cycles and the range of left-right tongue movements under nerve block. This may reflect a possible compensatory strategy of reaching the drinking spouts with an adjacent region of the tongue, instead of contacting the right or left spout with the ipsilateral tongue in Monkey R. We observed a decrease in the average speed (t-test, Monkey R: $p < 0.001$, Monkey Y: $p > 0.1$) and an increase in the variance of the speed (F-test $p < 0.001$) of tongue movement during drinking with nerve block.

Decreased directional tuning of MIo and SIo neurons. Loss of oral sensation also affected the proportion of directionally tuned neurons and the overall distribution of PDs, though the pattern of changes differed between subjects. Following nerve block, MIo and SIo showed significant decreases in the proportion of directionally modulated neurons across both tasks (Fig. 10A; Chi-square, MIo: $p < 0.001$, SIo: $p < 0.05$). To confirm this effect was not merely due to altered kinematics, we conducted parallel analyses using carefully subsampled trials with matched kinematic profiles from both control and nerve-blocked conditions. This controlled analysis confirmed the persistent decrease in directional tuning during nerve block (Figure 10 – figure supplement 1).

We further investigated whether neurons gaining or losing directional selectivity differed across regions. During feeding, MIo and SIo exhibited similar proportions of neurons gaining or losing directional tuning (Fig. 10B-top row, Chi-square, $p > 0.1$). The drinking task revealed subject-specific differences (Fig. 10B-bottom row): in Monkey R, significantly more neurons lost directional tuning in SIo compared to MIo ($p < 0.01$), while in Monkey Y, SIo showed a higher proportion of neurons gaining directional tuning than MIo ($p < 0.05$). Comparing across behaviors, Monkey R demonstrated consistent patterns of directional tuning changes (Chi-square, $p > 0.1$), whereas Monkey Y showed significantly higher percentages of neurons gaining directionality during drinking than feeding in both MIo and SIo ($p < 0.05$). Interestingly, there was a large proportion (40%) of SIo neurons in Monkey Y that gained directional tuning following sensory loss compared to Monkey R (8%) during drinking.

Nerve block significantly altered PD distributions during both tasks. During feeding, MIo neurons in both subjects exhibited a significant clockwise shift in mean PD toward the center (0°), resulting in more uniform distributions (Fig. 11A; circular k-test, $p < 0.01$). In contrast, SIo neurons showed subject-specific responses, with only Monkey R demonstrating a significant counterclockwise shift ($p < 0.05$). During drinking under nerve block, MIo neurons displayed subject-dependent directional shifts. In Monkey R, the proportion of neurons with rightward PDs decreased and increased in all other directions whereas Monkey Y showed the opposite with increased neurons with rightward PDs (Fig. 11B; Chi-square, Y: $p = 0.04$). Meanwhile, SIo neurons consistently shifted rightward in both animals (Chi-square, R: $p = 0.02$), suggesting differential regional responses to peripheral deafferentation.

Separation of neural population trajectories was reduced in MIo. Disruption of tactile inputs during feeding had opposite effects on MIo and SIo. Neural population trajectories in MIo showed reduced inter-trajectory distances during nerve block compared to control conditions (Fig. 12, left, t-test, $p < 0.05$ in >89% of pairs), whereas SIo exhibited increased inter-trajectory distances (Fig. 12 top right, t-test, $p < 0.05$ in >75% of pairs). In drinking, inter-trajectory distances in both MIo and SIo were significantly reduced across all pairs (two-tailed t-test, $p < 0.01$) except middle-right in Monkey R's SIo neurons ($p>0.1$).

The effects of nerve block on the distance travelled by population trajectories were inconsistent across subjects and behavior. Following nerve block, the total distance travelled by SIo trajectories became longer in different behaviors for a specific subject (t-test, Monkey R feeding: $p < 0.001$; Monkey Y drinking: $p < 0.05$). In contrast, MIo trajectories became shorter in drinking (Monkey Y, $p < 0.01$).

<u>Population decoding of tongue direction.</u> To assess directional information within population activity further, we implemented two decoding approaches to predict tongue movement direction from neuronal spiking patterns: k-nearest neighbor (KNN) classifier and long short-term memory (LSTM) neural network. Consistent with previous study on a cued tongue protrusion task (Arce et al., 2013), we found that the 3D direction of tongue movements in naturalistic behaviors could be decoded from simultaneously recorded MIo and SIo populations. The KNN classifier successfully decoded 3D tongue movement direction above chance level across behaviors and experimental conditions (Fig. 13A). Results of analyses using multiple linear regression model with interactions revealed several key factors affecting decoder performance: behavior type ($p < 0.001$, drinking outperformed feeding by 11%), cortical region ($p < 0.001$, MIo exceeded SIo by 13%), and inter-subject variability with behavior ($p < 0.001$, 12% higher for Monkey R during drinking, comparable accuracy during feeding). Notably, disrupting tactile sensation through nerve block did not significantly impair KNN classifier performance ($p > 0.1$). The results using LSTM were different from that of KNN; decoding tongue direction using LSTM showed substantially higher performance when using MIo neural activity (mean $R^2 \pm 1$ SD: control: 0.46-0.81 ± 0.1, nerve block: 0.26-0.7 ± 0.1) compared to SIo (mean $R^2 \pm 1$ SD: control: 0.12-0.43 ± 0.1, nerve block: 0.05-0.17 ± 0.07) across all experimental conditions (Fig. 13B, t-test, $p < 0.001$). This regional difference became particularly pronounced during nerve block, where SIo decoding accuracy decreased substantially more than MIo, suggesting differential reliance on tactile feedback between these cortical regions. Combining MIo and SIo showed significantly better decoder performance compared to performance using neuronal populations separately (mean $R^2 \pm 1$ SD: control: 0.78-0.92 ± 0.05, nerve block: 0.58-0.91 ± 0.05, $p < 0.001$) in feeding, but not drinking. To address the potential confound of varying population sizes between MIo and SIo, we standardized comparisons by downsampling all populations to match our smallest recorded group (N = 28 neurons). Decoding accuracy improved by up to 10% when using all neurons in MIo or SIo compared to using subsamples of neurons. Decoding using LSTM showed consistently higher accuracies in feeding compared to drinking regardless of the length of intervals used (100 ms, 500 ms), behavioral window (± 500 ms relative to minimum protrusion, between maximal protrusions), and directional angles (actual vs. {-45, 0, 45}). These results suggest that continuous and non-linear decoding is better suited for feeding than drinking behavior.

Discussion

Our study investigated the representation of 3D directional information in MIo and SIo during natural feeding and drinking behaviors, and how cortical representations change when tactile sensation is disrupted. By simultaneously recording large-scale cortical activity and 3D tongue kinematics, we revealed a nuanced neural encoding of tongue movement direction that varies systematically across cortical regions, behaviors, and sensory feedback conditions. We found that a substantial proportion of neurons exhibit directional tuning characterized by diverse tuning curve properties (PD, tuning shape, modulation depth). Neural population trajectories demonstrated distinct patterns across different movement directions. Directional tuning in both individual- and population-level is more robust in MIo. Following sensory loss, alterations in tongue kinematics were accompanied by changes in directional information in MIo and SIo, manifesting as modifications in both individual neuron tuning characteristics and the broader dynamics of population-level neural activity.

Differences across behaviors. In the present study, results from the more natural drinking are consistent with previous findings that MIo and SIo encode tongue direction during a trained protrusion task (Murray and Sessle, 1992; Sessle et al., 2005a; Arce et al., 2013). Our study extends this knowledge by investigating the dynamics of directional tuning of individual and population of neurons in OSMCx to 3D tongue direction during naturalistic behaviors. Unlike previous similar studies, the monkeys were not trained to reach specific targets and were instead allowed to eat and drink relatively naturally. By comparing two naturalistic behaviors, we found that the directional information in OSMcx was higher in feeding than in the drinking task, as seen in higher proportion of directionally tuned neurons, cumulative variance explained by latent factors, and decoding accuracies. That directional tuning is modifiable is consistent with previous findings in primate motor cortex where directional tuning was modulated by movement parameters such as speed, posture, distance (Aflalo and Graziano, 2006) and by varying task contexts such as availability of prior information (Rickert et al., 2009), individual vs. segmented arm movements (Ben-Shaul et al., 2004) , one- vs two-target reaching (Ebina et al., 2024). A high degree of similarity in neural modes have been reported across different wrist tasks in 1-D and 2D (Gallego et al., 2018). This suggests that in our study, feeding and drinking may reflect more distinct biomechanical constraints and sensorimotor requirements compared to the wrist tasks. In feeding, the tongue moves in varied directions to position the food between left-right toothrows during chewing, whereas in the drinking task, the tongue moves to discrete and fixed spout locations. Additionally, feeding and drinking engage the jaw differently. During feeding, the jaw moves more extensively and in multiple directions, while jaw movements during drinking are smaller and primarily vertical. Lastly, the tongue-jaw coordination differs between tasks; maximum tongue protrusion coincides with maximum gape in drinking but with minimum gape in the feeding behavior (Laurence-Chasen et al., 2022; Punacha et al., 2024). Indeed, MIo

trajectories' predominant latent factor contained directional information in the feeding task, resembling superior-inferior directional components which rotated in opposite directions. In contrast, MIo trajectories in drinking exhibited a consistent rotational direction regardless of spout location (Fig. 7). This may reflect a predominant non-directional information such as condition-independent time-varying spiking activity during drinking (Kaufman et al., 2013; Kobak et al., 2016; Arce-McShane et al., 2023).

Comparison between MIo and SIo. Directional tuning of neurons during feeding showed a notable disparity between MIo and SIo, suggesting that MIo carries more robust directional information for tongue movements in feeding tasks. The similar proportions of directionally tuned MIo and SIo neurons in the drinking task studied here were consistent with previous findings (Arce et al., 2013). At the population level, MIo trajectories showed more consistent rotational patterns and greater inter-trajectory separation than those in SIo. Consistent with results from previous studies (Michaels et al., 2016; Seely et al., 2016; Russo et al., 2018), MIo trajectories exhibited low tanging and smoother dynamics than SIo trajectories. These may suggest that the low tangling in MIo confers noise robustness while the higher tangling in SIo reflects variability in the tactile signals received by SIo during feeding. Consistent with our previous study (Laurence-Chasen et al., 2023), decoding from MIo yielded higher accuracies than from SIo in both behaviors. These results support the well-established role of MIo in the control of movement parameters, especially direction. Varying tongue shape, tongue's contact with varying bolus properties (size and texture) and other oral structures (palate, teeth) may weaken the directional signal contained in SIo activity. Thus, small differences in tongue kinematics might create large differences in sensory signals across trials. When looking at trial-averaged signals, this natural variability could make the neural response patterns appear less precise or specific than they are. These are consistent with our findings that for both tasks, spiking variability was higher in SIo, and that the variance accounted for was lower in SIo population activity compared to MIo.

Laterality in OSMCx. Similar to previous results in arm motor cortex (Lillicrap and Scott, 2013), we observed non-uniform PD distributions consistent with the frequency distribution of tongue movements, suggesting that neural populations contain information that reflects the anatomical constraints of the tongue. The highest frequency of both observed directions and directional tuning peaks were in the anterior and superior directions. We additionally found that the peak of the PD distribution, especially in feeding, coincides with leftward tongue movements, suggesting the presence of laterality in the PDs of OSMCx neurons. Previous results in humans examined using fMRI reported that hemispheric differences in sensorimotor activity during voluntary tongue movements are related to the preferred chew side (Shinagawa et al., 2003). This was not the case in our study as the preferred chew side was the same for both monkeys (i.e., right side), despite differences in the predominant PD. It is possible that the difference between the two subjects is related to the difference in recording locations, with Monkey Y's being more lateral

and therefore closer to the swallow area of the cortex than Monkey R's (Supplementary file 1, Fig. 1). Monkey Y had a higher proportion of neurons that were tuned to tongue direction during feeding compared to Monkey R (Figure 3 – figure supplement 2), but fewer during drinking. An avenue for further study could be a unilateral nerve block on the preferred side to measure how the unaffected side of the tongue compensates for the lack of sensation in the affected side. A previous study found that unilateral lingual nerve transection in pigs alters the coordination of the ipsilateral tongue side during chewing (Montuelle et al., 2020). The tongue is a complex group of muscles, with intrinsic muscles primarily contributing to the shape of the tongue and extrinsic muscles contributing more to the positioning of the tongue. Therefore, it is possible that the neurons which are strongly tuned to tongue direction have direct connections to the extrinsic muscles on the ipsilateral side. Looking at how each side of the tongue responds independently to unilateral nerve block, and how this interacts with directional preference may give us more information about how the unique structure of the tongue is coordinated.

Role of tactile feedback. Previously, we reported that the administration of bilateral nerve block to the sensory branches of the trigeminal nerve impaired feeding performance and tongue jaw coordination (Laurence-Chasen et al., 2022). The present study extends these findings by showing that directional movement of the tongue (*kinematics*) and the directional information in both MIo and SIo are also affected by the loss of tactile inputs from the tongue and other structures of the oral cavity (e.g., palate, teeth, gingiva). These findings highlight the critical role of sensory information in sensorimotor control in general (Dadarlat et al., 2015; Delhaye et al., 2018) and in the representation and computation of directional signals for controlling tongue movements. MIo and SIo neurons, which respond to tactile and proprioceptive inputs from the tongue (Huang et al., 1989; Lin et al., 1994b; Toda and Taoka, 2002, 2004, 2006; Arce et al., 2013; Cerkevich et al., 2014), use sensory information to plan and adjusts tongue movements to achieve contact with the spout or position the bolus appropriately at different stages of the feeding sequence. Without tactile feedback, subjects may rely on alternative sensory cues like taste for locating the spout or bolus (Todrank and Bartoshuk, 1991) . In a recent optogenetic inhibition study on licking in mice, it was found that the tongue/jaw regions of the somatosensory cortex were necessary for proper tongue targeting but not for the core motor capabilities of the tongue (Xu et al., 2022). The reduced range of tongue motion we observed likely stems from sensory loss rather than motor impairment. While our experimental setup did not eliminate visual feedback that monkeys might use to readjust tongue position in the drinking task, oral sensory loss alone had a significant effect on the monkeys' performance in feeding, as the tongue was out of sight within the oral cavity.

Individual differences were notable in our study possibly due to differences in the electrode array placement or compensatory strategies. This individual variability suggests that studying additional subjects would provide valuable insights into how OSMCx adapts following sensory disruption. In our study, head position and hand movement were restrained, to eliminate

contributions of hand-to-mouth movements when handling food or drink. The hand and orofacial cortical areas are anatomically adjacent and highly interconnected (Forrester and Rodriguez, 2015), and researchers have found a neural region in mice that coordinates hand-to-mouth movements during natural feeding (An et al., 2022). Truly natural feeding would involve holding food up to the mouth, as well as free head movement, which would make tracking of the marker positions difficult under this experimental setup. Advances in tracking tongue movements would be necessary to study more complex feeding sequences.

Clinical implications

This study offers new information about the important role of sensorimotor integration in controlling tongue direction during natural behaviors. There is a high degree of directional information contained in the spiking activity of the orofacial cortex, especially in the motor areas. The effect of the bilateral nerve block serves to enhance our understanding of the processes affected by oral sensorimotor dysfunctions such as trigeminal neuropathies. It demonstrates the importance of oral sensation for supporting the full range of directional motion but also shows that significant directional information can be extracted even in the absence of tactile feedback. This type of knowledge can inform the diagnosis and rehabilitation of orolingual dysfunctions, following stroke or glossectomy. There have also been advancements in brain-computer interface (BCI) by decoding the real-time signals of arm region of the motor cortex to control prosthetic arm movement (Collinger et al., 2013; Vilela and Hochberg, 2020) or muscle stimulation (Ethier and Miller, 2015), as well as efforts to restore sensory feedback by stimulating correct areas of somatosensory cortex in response to sensors on a prosthetic (Tabot et al., 2013; Flesher et al., 2021). That the OSMCx, particularly MIo, can rapidly decode tongue direction during natural behaviors is significant for developing neuroprosthetic control or soft prosthetics.

Ethics statement

Experiments were performed in the University of Chicago XROMM Facility. All protocols were approved by the University of Chicago Animal Care and Use Committee and complied with the National Institutes of Health Guide for the Care and Use of Laboratory Animals.

Funding information

This research was supported by National Institutes of Health grants from the National Institute on Aging, Grant Number: R01AG069227 (to F.I.A-M, PI) and the National Institute of Dental and Craniofacial Research, Grant Number: R01DE027236 (to F.I.A-M, PI). The content is solely the responsibility of the authors and does not necessarily represent the official views of the National Institutes of Health.

The funders had no role in study design, data collection and interpretation, or the decision to submit the work for publication.

Author contributions

Victoria B. Hosack: data analysis, writing – original draft, writing – review and editing, visualization.

Fritzie I. Arce-McShane: conceptualization, methodology, investigation, writing – review and editing, supervision, project administration, funding acquisition.

Acknowledgements

We thank J.D. Laurence-Chasen for data collection and software, Christina Hahn for assistance with LSTM analysis, as well as all members of the Arce-McShane Lab past and present, including Rebecca Junod, Hernando Fereira, Derrick Tang, Emma Lesser, Jared Luckas, Tricia Nicholson, Eric Hosack, for assistance with data collection and processing.

References

Aflalo TN, Graziano MS (2006) Partial tuning of motor cortex neurons to final posture in a free-moving paradigm. Proc Natl Acad Sci USA 103:2909–2914 Available at: http://www.ncbi.nlm.nih.gov/pubmed/16473936.

Ajemian R, Bullock D, Grossberg S (2000) Kinematic Coordinates In Which Motor Cortical Cells Encode Movement Direction. J Neurophysiol 84:2191–2203 Available at: https://doi.org/10.1152/jn.2000.84.5.2191.

An X, Matho K, Li Y, Mohan H, Xu XH, Whishaw IQ, Kepecs A, Huang ZJ (2022) A cortical circuit for orchestrating oromanual food manipulation. bioRxiv.

Arce F, Novick I, Mandelblat-Cerf Y, Israel Z, Ghez C, Vaadia E (2010) Combined adaptiveness of specific motor cortical ensembles underlies learning. Journal of Neuroscience 30.

Arce FI, Lee J-C, Ross CF, Sessle BJ, Hatsopoulos NG (2013) Directional information from neuronal ensembles in the primate orofacial sensorimotor cortex. J Neurophysiol 110:1357–1369 Available at: http://dx.doi.org/10.1152/jn.00144.2013.

Arce-McShane FI, Sessle BJ, Ram Y, Ross CF, Hatsopoulos NG (2023) Multiple regions of primate orofacial sensorimotor cortex encode bite force and gape. Front Syst Neurosci.

Avivi-Arber L, Sessle BJ (2017) Jaw sensorimotor control in healthy adults and effects of ageing. J Oral Rehabil 45:50–80 Available at: http://dx.doi.org/10.1111/joor.12554.

Bach-y-Rita P, Kaczmarek KA, Tyler ME, Garcia-Lara J (1998) Form perception with a 49-point electrotactile stimulus array on the tongue: a technical note. J Rehabil Res Dev 35:427–430 Available at: https://www.ncbi.nlm.nih.gov/pubmed/10220221.

Ben-Shaul Y, Drori R, Asher I, Stark E, Nadasdy Z, Abeles M (2004) Neuronal Activity in Motor Cortical Areas Reflects the Sequential Context of Movement. J Neurophysiol 91:1748–1762 Available at: https://doi.org/10.1152/jn.00957.2003.

Berens P (2009) **CircStat** : A *MATLAB* Toolbox for Circular Statistics. J Stat Softw 31.

Brainerd EL, Baier DB, Gatesy SM, Hedrick TL, Metzger KA, Gilbert SL, Crisco JJ (2010) X-ray reconstruction of moving morphology (XROMM): precision, accuracy and applications in comparative biomechanics research. J Exp Zool A Ecol Genet Physiol 313A:262–279 Available at: http://dx.doi.org/10.1002/jez.589.

Cerkevich CM, Qi H-X, Kaas JH (2014) Corticocortical projections to representations of the teeth, tongue, and face in somatosensory area 3b of macaque monkeys. J Comp Neurol 522:546–572.

Churchland MM et al. (2010) Stimulus onset quenches neural variability: a widespread cortical phenomenon. NatNeurosci 13:369–378 Available at: http://www.ncbi.nlm.nih.gov/pubmed/20173745.

Churchland MM, Cunningham JP, Kaufman MT, Foster JD, Nuyujukian P, Ryu SI, Shenoy K V (2012) Neural population dynamics during reaching. Nature 487:51–56 Available at: https://doi.org/10.1038/nature11129.

Collinger JL, Wodlinger B, Downey JE, Wang W, Tyler-Kabara EC, Weber DJ, McMorland AJC, Velliste M, Boninger ML, Schwartz AB (2013) High-performance neuroprosthetic control by an individual with tetraplegia. Lancet 381:557–564 Available at: https://pubmed.ncbi.nlm.nih.gov/23253623.

Cowley BR, Kaufman MT, Butler ZS, Churchland MM, Ryu SI, Shenoy K V, Yu BM (2013) DataHigh: graphical user interface for visualizing and interacting with high-dimensional neural activity. J Neural Eng 10:066012 Available at: https://dx.doi.org/10.1088/1741-2560/10/6/066012.

Dadarlat MC, O'Doherty JE, Sabes PN (2015) A learning-based approach to artificial sensory feedback leads to optimal integration. Nat Neurosci 18:138–144 Available at: https://doi.org/10.1038/nn.3883.

Delhaye BP, Long KH, Bensmaia SJ (2018) Neural Basis of Touch and Proprioception in Primate Cortex. In: Comprehensive Physiology, pp 1575–1602 Available at: https://doi.org/10.1002/cphy.c170033.

Dickey AS, Suminski A, Amit Y, Hatsopoulos NG (2009) Single-unit stability using chronically implanted multielectrode arrays. JNeurophysiol 102:1331–1339 Available at: http://www.ncbi.nlm.nih.gov/pubmed/19535480.

Ebina T, Sasagawa A, Hong D, Setsuie R, Obara K, Masamizu Y, Kondo M, Terada S-I, Ozawa K, Uemura M, Takaji M, Watakabe A, Kobayashi K, Ohki K, Yamamori T, Murayama M, Matsuzaki M (2024) Dynamics of directional motor tuning in the primate premotor and primary motor cortices during sensorimotor learning. Nat Commun 15:7127 Available at: https://doi.org/10.1038/s41467-024-51425-3.

Ethier C, Miller LE (2015) Brain-controlled muscle stimulation for the restoration of motor function. Neurobiol Dis 83:180–190 Available at: https://pubmed.ncbi.nlm.nih.gov/25447224.

Feilich K, Orsbon C, Gidmark N, Ross C (2021) Twist and chew: three-dimensional tongue kinematics during chewing in macaque primates. Biol Lett 17.

Flesher SN, Downey JE, Weiss JM, Hughes CL, Herrera AJ, Tyler-Kabara EC, Boninger ML, Collinger JL, Gaunt RA (2021) A brain-computer interface that evokes tactile sensations improves robotic arm control. Science 372:831–836 Available at: https://pubmed.ncbi.nlm.nih.gov/34016775.

Forrester GS, Rodriguez A (2015) Slip of the tongue: Implications for evolution and language development. Cognition 141:103–111 Available at: http://dx.doi.org/10.1016/j.cognition.2015.04.012.

Gallego JA, Perich MG, Naufel SN, Ethier C, Solla SA, Miller LE (2018) Cortical population activity within a preserved neural manifold underlies multiple motor behaviors. Nat Commun 9:4233 Available at: http://dx.doi.org/10.1038/s41467-018-06560-z.

Georgopoulos AP, Kettner RE, Schwartz AB (1988) Primate Motor Cortex and Free Arm Movements to Visual Targets in Three-Dimensional Space. II. Coding of the Direction of Movement by a Neuronal Population. JNeurosci 8:2928–2937.

Georgopoulos AP, Merchant H, Naselaris T, Amirikian B (2007) Mapping of the preferred direction in the motor cortex. Proc Natl Acad Sci U S A 104:11068–11072 Available at: http://dx.doi.org/10.1073/pnas.0611597104.

Glaser JI, Benjamin AS, Chowdhury RH, Perich MG, Miller LE, Kording KP (2020) Machine Learning for Neural Decoding. eNeuro 7:ENEURO.0506-19.2020 Available at: http://www.eneuro.org/content/7/4/ENEURO.0506-19.2020.abstract.

Hahn C, Arce-McShane FI (2024) Impact of nerve block on the cortical decoding of tongue movements across axes of motion and marker regions. In: Program No. LBA005.27. 2024 Neuroscience Meeting Planner. Chicago, IL: Society for Neuroscience.

Hiiemae KM, Palmer JB (2003) Tongue Movements in Feeding and Speech. Critical Reviews in Oral Biology & Medicine 14:413–429 Available at: https://doi.org/10.1177/154411130301400604.

Hochreiter S, Schmidhuber J (1997) Long Short-Term Memory. Neural Comput 9:1735–1780.

Horrocks EAB, Rodrigues FR, Saleem AB (2024) Flexible neural population dynamics govern the speed and stability of sensory encoding in mouse visual cortex. Nat Commun 15:6415 Available at: https://doi.org/10.1038/s41467-024-50563-y.

Huang CS, Hiraba H, Sessle BJ (1989) Input-output relationships of the primary face motor cortex in the monkey (Macaca fascicularis). J Neurophysiol 61:350–362 Available at: https://doi.org/10.1152/jn.1989.61.2.350.

Kaufman MT, Churchland MM, Shenoy K V (2013) The roles of monkey M1 neuron classes in movement preparation and execution. J Neurophysiol 110:817–825 Available at: https://doi.org/10.1152/jn.00892.2011.

Knörlein BJ, Baier DB, Gatesy SM, Laurence-Chasen JD, Brainerd EL (2016) Validation of XMALab software for marker-based XROMM. Journal of Experimental Biology.

Kobak D, Brendel W, Constantinidis C, Feierstein CE, Kepecs A, Mainen ZF, Qi X-L, Romo R, Uchida N, Machens CK (2016) Demixed principal component analysis of neural population data. Elife 5:1–36 Available at: https://elifesciences.org/articles/10989.

Lamm NC, De Felice A, Cargan A (2005) Effect of tactile stimulation on lingual motor function in pediatric lingual dysphagia. Dysphagia 20:311–324 Available at: http://dx.doi.org/10.1007/s00455-005-0060-7.

Laurence-Chasen JD, Arce-McShane FI, Hatsopoulos NG, Ross CF (2022) Loss of oral sensation impairs feeding performance and consistency of tongue-jaw coordination. J Oral Rehabil 49:806–816 Available at: https://pubmed.ncbi.nlm.nih.gov/35514258.

Laurence-Chasen JD, Manafzadeh AR, Hatsopoulos NG, Ross CF, Arce-McShane FI (2020) Integrating XMALab and DeepLabCut for high-throughput XROMM. J Exp Biol 223:jeb226720 Available at: https://pubmed.ncbi.nlm.nih.gov/32665442.

Laurence-Chasen JD, Ross CF, Arce-McShane FI, Hatsopoulos NG (2023) Robust cortical encoding of 3D tongue shape during feeding in macaques. Nat Commun 14:2991 Available at: https://pubmed.ncbi.nlm.nih.gov/37225708.

Lillicrap TP, Scott SH (2013) Preference Distributions of Primary Motor Cortex Neurons Reflect Control Solutions Optimized for Limb Biomechanics. Neuron 77:168–179 Available at: https://doi.org/10.1016/j.neuron.2012.10.041.

Lin LD, Murray GM, Sessle BJ (1994a) Functional properties of single neurons in the primate face primary somatosensory cortex. I. Relations with trained orofacial motor behaviors. J Neurophysiol 71:2377–2390 Available at: http://www.ncbi.nlm.nih.gov/pubmed/7931522.

Lin LD, Murray GM, Sessle BJ (1994b) Functional properties of single neurons in the primate face primary somatosensory cortex. I. Relations with trained orofacial motor behaviors. J Neurophysiol 71:2377–2390 Available at: http://www.ncbi.nlm.nih.gov/pubmed/7931522.

Lozano CA, Kaczmarek KA, Santello M (2009) Electrotactile stimulation on the tongue: Intensity perception, discrimination, and cross-modality estimation. Somatosens Mot Res 26:50–63 Available at: http://dx.doi.org/10.1080/08990220903158797.

Mathis A, Mamidanna P, Cury KM, Abe T, Murthy VN, Mathis MW, Bethge M (2018) DeepLabCut: markerless pose estimation of user-defined body parts with deep learning. Nat Neurosci 21:1281–1289.

Michaels JA, Dann B, Scherberger H (2016) Neural Population Dynamics during Reaching Are Better Explained by a Dynamical System than Representational Tuning. PLoS Comput Biol 12:e1005175- Available at: https://doi.org/10.1371/journal.pcbi.1005175.

Montuelle SJ, Olson RA, Curtis H, Williams SH (2020) Unilateral lingual nerve transection alters jaw-tongue coordination during mastication in pigs. J Appl Physiol (1985) 128:941–951 Available at: https://pubmed.ncbi.nlm.nih.gov/32191597.

Murray GM, Sessle BJ (1992) Functional properties of single neurons in the face primary motor cortex of the primate. III. Relations with different directions of trained tongue protrusion. J Neurophysiol 67:775–785 Available at: http://dx.doi.org/10.1152/jn.1992.67.3.775.

Prud'homme MJ, Kalaska JF (1994) Proprioceptive activity in primate primary somatosensory cortex during active arm reaching movements. J Neurophysiol 72:2280–2301 Available at: http://dx.doi.org/10.1152/jn.1994.72.5.2280.

Punacha S, Huang K, Arce-McShane FI (2024) Effects of healthy aging on tongue-jaw kinematics during feeding behavior in rhesus macaques. bioRxiv:2024.07.31.605680 Available at: http://biorxiv.org/content/early/2024/08/03/2024.07.31.605680.abstract.

Rickert J, Riehle A, Aertsen A, Rotter S, Nawrot MP (2009) Dynamic Encoding of Movement Direction in Motor Cortical Neurons. The Journal of Neuroscience 29:13870 Available at: http://www.jneurosci.org/content/29/44/13870.abstract.

Russo AA, Bittner SR, Perkins SM, Seely JS, London BM, Lara AH, Miri A, Marshall NJ, Kohn A, Jessell TM, Abbott LF, Cunningham JP, Churchland MM (2018) Motor Cortex Embeds Muscle-like Commands in an Untangled Population Response. Neuron 97:953-966.e8 Available at: http://dx.doi.org/10.1016/j.neuron.2018.01.004.

Santhanam G, Yu BM, Gilja V, Ryu SI, Afshar A, Sahani M, Shenoy K V (2009) Factor-Analysis Methods for Higher-Performance Neural Prostheses. J Neurophysiol 102:1315–1330 Available at: https://doi.org/10.1152/jn.00097.2009.

Schwartz AB, Kettner RE, Georgopoulos AP (1988a) Primate motor cortex and free arm movements to visual targets in three-dimensional space. I. relations between single cell discharge and direction of movement. JNeurosci 8:2913–2927.

Schwartz AB, Kettner RE, Georgopoulos AP (1988b) Primate motor cortex and free arm movements to visual targets in three-dimensional space. I. relations between single cell discharge and direction of movement. JNeurosci 8:2913–2927.

Seely JS, Kaufman MT, Ryu SI, Shenoy K V, Cunningham JP, Churchland MM (2016) Tensor Analysis Reveals Distinct Population Structure that Parallels the Different Computational Roles of Areas M1 and V1. PLoS Comput Biol 12:e1005164- Available at: https://doi.org/10.1371/journal.pcbi.1005164.

Sessle BJ, Yao D, Nishiura H, Yoshino K, Lee J, Martin RE, Murray GM (2005a) Properties and plasticity of the primate somatosensory and motor cortex related to orofacial sensorimotor function. Clin Exp Pharmacol Physiol 32:109–114 Available at: http://dx.doi.org/10.1111/j.1440-1681.2005.04137.x.

Sessle BJ, Yao D, Nishiura H, Yoshino K, Lee JC, Martin RE, Murray GM, Yao B, Nishiura H, Yoshino K, Lee JC, Martin RE, Murray GM (2005b) Properties and plasticity of the primate somatosensory and motor cortex related to orofacial sensorimotor function. Clin Exp Pharmacol Physiol 32:109–114 Available at: http://www.ncbi.nlm.nih.gov/pubmed/15730444.

Shinagawa H, Ono T, Ishiwata Y, Honda E, Sasaki T, Taira M, Iriki A, Kuroda T (2003) Hemispheric Dominance of Tongue Control Depends on the Chewing-side Preference. J Dent Res 82:278–283.

Smith JH, Cutrer FM (2011) Numbness matters: A clinical review of trigeminal neuropathy. Cephalalgia 31:1131–1144 Available at: http://dx.doi.org/10.1177/0333102411411203.

Tabot GA, Dammann JF, Berg JA, Tenore F V, Boback JL, Vogelstein RJ, Bensmaia SJ (2013) Restoring the sense of touch with a prosthetic hand through a brain interface. Proc Natl Acad Sci U S A 110:18279–18284 Available at: https://pubmed.ncbi.nlm.nih.gov/24127595.

Takizawa C, Gemmell E, Kenworthy J, Speyer R (2016) A Systematic Review of the Prevalence of Oropharyngeal Dysphagia in Stroke, Parkinson's Disease, Alzheimer's Disease, Head Injury, and Pneumonia. Dysphagia 31:434–441 Available at: http://dx.doi.org/10.1007/s00455-016-9695-9.

Toda T, Taoka M (2002) Hierarchical somesthetic processing of tongue inputs in the postcentral somatosensory cortex of conscious macaque monkeys. Exp Brain Res 147:243–251 Available at: http://www.ncbi.nlm.nih.gov/pubmed/12410339.

Toda T, Taoka M (2004) Converging patterns of inputs from oral structures in the postcentral somatosensory cortex of conscious macaque monkeys. Exp Brain Res 158:43–49 Available at: http://www.ncbi.nlm.nih.gov/pubmed/15014923.

Toda T, Taoka M (2006) Postcentral neurons with covert receptive fields in conscious macaque monkeys: their selective responsiveness to simultaneous two-point stimuli applied to discrete oral portions. Exp Brain Res 168:303–306 Available at: http://www.ncbi.nlm.nih.gov/pubmed/16307237.

Todrank J, Bartoshuk LM (1991) A taste illusion: Taste sensation localized by touch. Physiol Behav 50:1027–1031 Available at: https://www.sciencedirect.com/science/article/pii/003193849190432N.

Vilela M, Hochberg LR (2020) Applications of brain-computer interfaces to the control of robotic and prosthetic arms. In: Handbook of Clinical Neurology, pp 87–99.

Xu D, Dong M, Chen Y, Delgado AM, Hughes NC, Zhang L, O'Connor DH (2022) Cortical processing of flexible and context-dependent sensorimotor sequences. Nature 603:464–469 Available at: https://pubmed.ncbi.nlm.nih.gov/35264793.

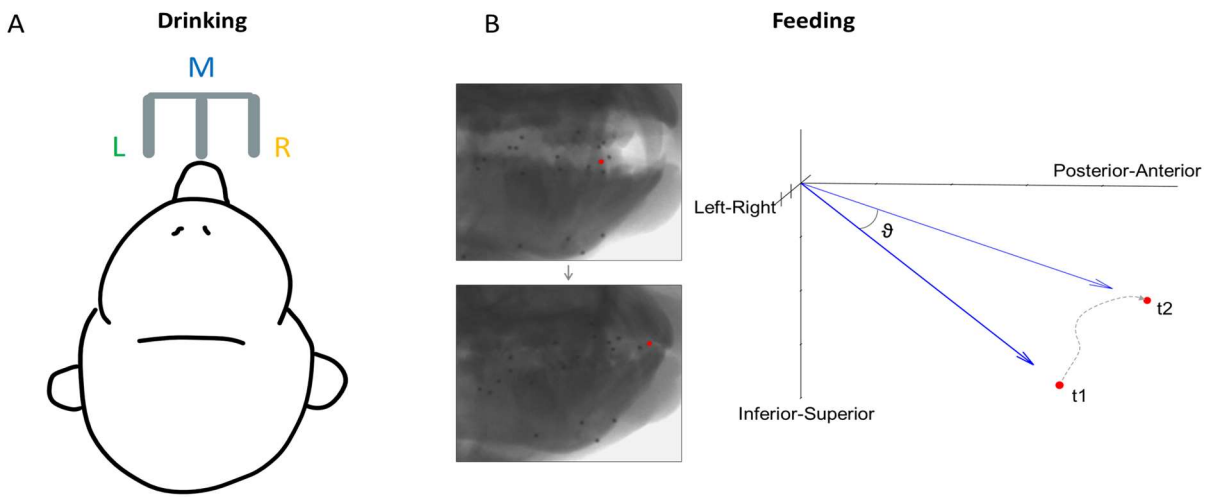

Figure 1. *Direction of tongue motion in each behavioral task.* ***(A)*** *Schematic of the location of three spouts, left (L), middle (M), and right (R), for the drinking task. Tongue direction was categorized based on spout location.* ***(B)*** *Calculation of 3D tongue direction during feeding. ϑ is the instantaneous 3D direction of the tongue tip over a 100 ms interval between its positions at t1 and t2, where t1 = 0 and t2 = t1 + 100. The dotted line shows the actual trajectory during this interval.*

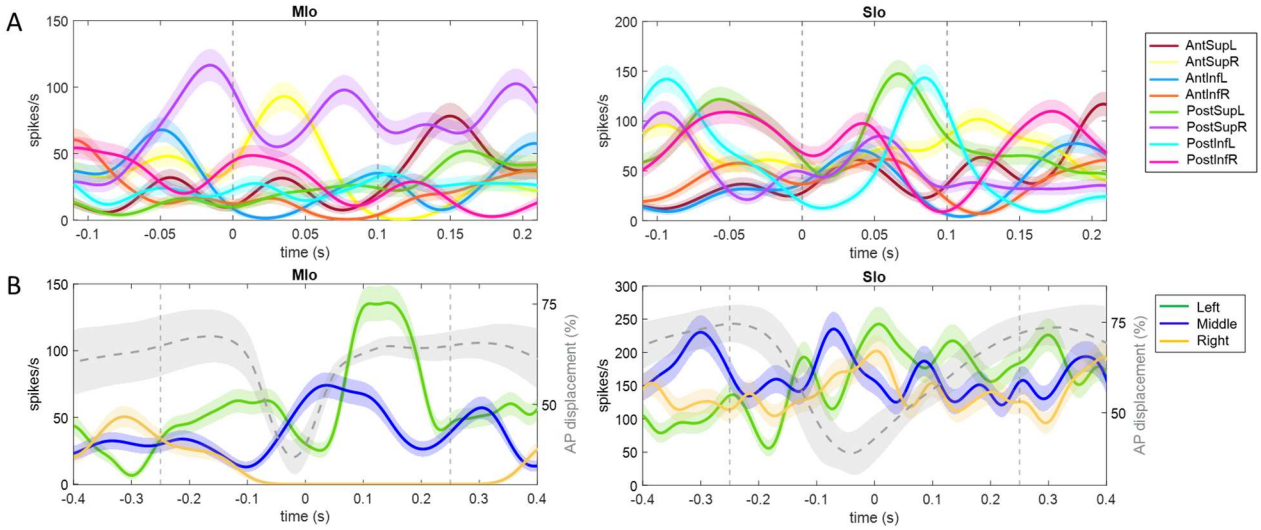

Figure 2. *Examples of single neuron activity in relation to tongue direction.* ***(A)*** *Each peri-event time histogram (PETH and ±1 SE, smoothed by a 25-ms Gaussian kernel) corresponds to spiking activity for a specific range of tongue direction for feeding trials. Dashed lines indicate 100-ms interval used for calculating the tongue direction.* ***(B)*** *PETHs for drinking trials with the same spout, centered at the point of minimum protrusion of the tongue (0-s). Percent tongue displacement along the anterior-posterior axis is shown in grey, with shaded area representing ±1 SD. Vertical lines indicate 500-ms interval used for tuning analysis.*

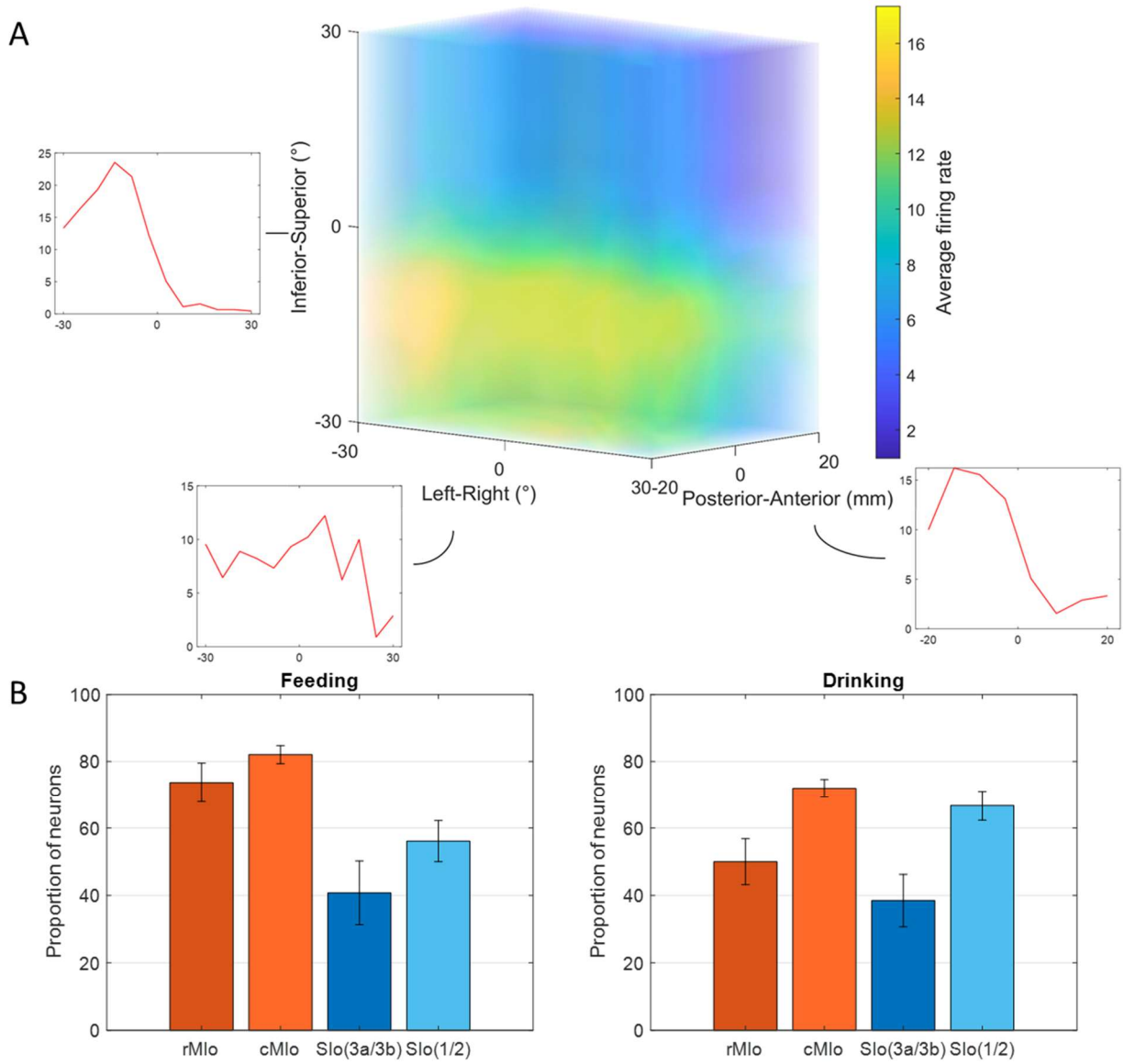

Figure 3. *Directional tuning of neurons during control tasks.* ***(A)*** *3D firing rate map of a neuron in MIo during feeding. Smaller inset plots are 1D tuning curves across each axis.* ***(B)*** *Percentage of neurons tuned to direction, combined for both subjects. Recordings were taken from four areas of the OSMCx: rMIo - rostral M1, cMIo - caudal M1, SIo(3a/3b) - area 3a/3b, and SIo(1/2) - area 1/2. Error bars represent ±1 SE.*

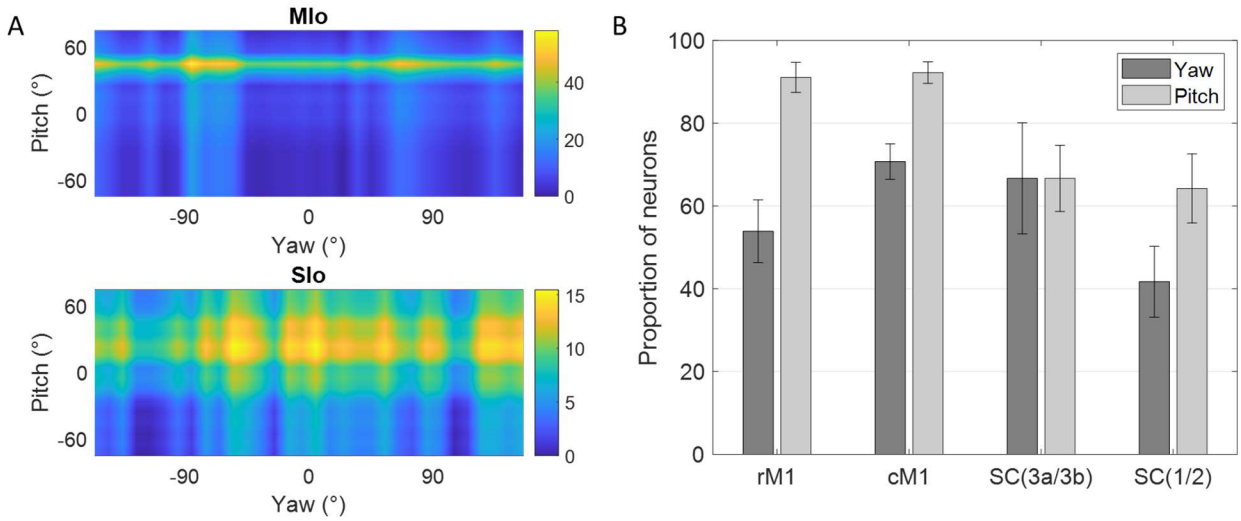

***Figure 4**. Directional tuning to yaw and pitch during feeding. **(A)** Firing rate maps of a neuron in MIo and in SIo across yaw and pitch angles. Firing rates were averaged across all 100 ms feeding intervals within a 10° range. **(B)** Proportion of neurons tuned to yaw and pitch, combined for both subjects. Recordings were taken from four areas of the OSMCx: rM1 - rostral M1, cM1 - caudal M1, SC(3a/3b) - area 3a/3b, and SC(1/2) - area 1/2. Error bars represent ±1 SE.*

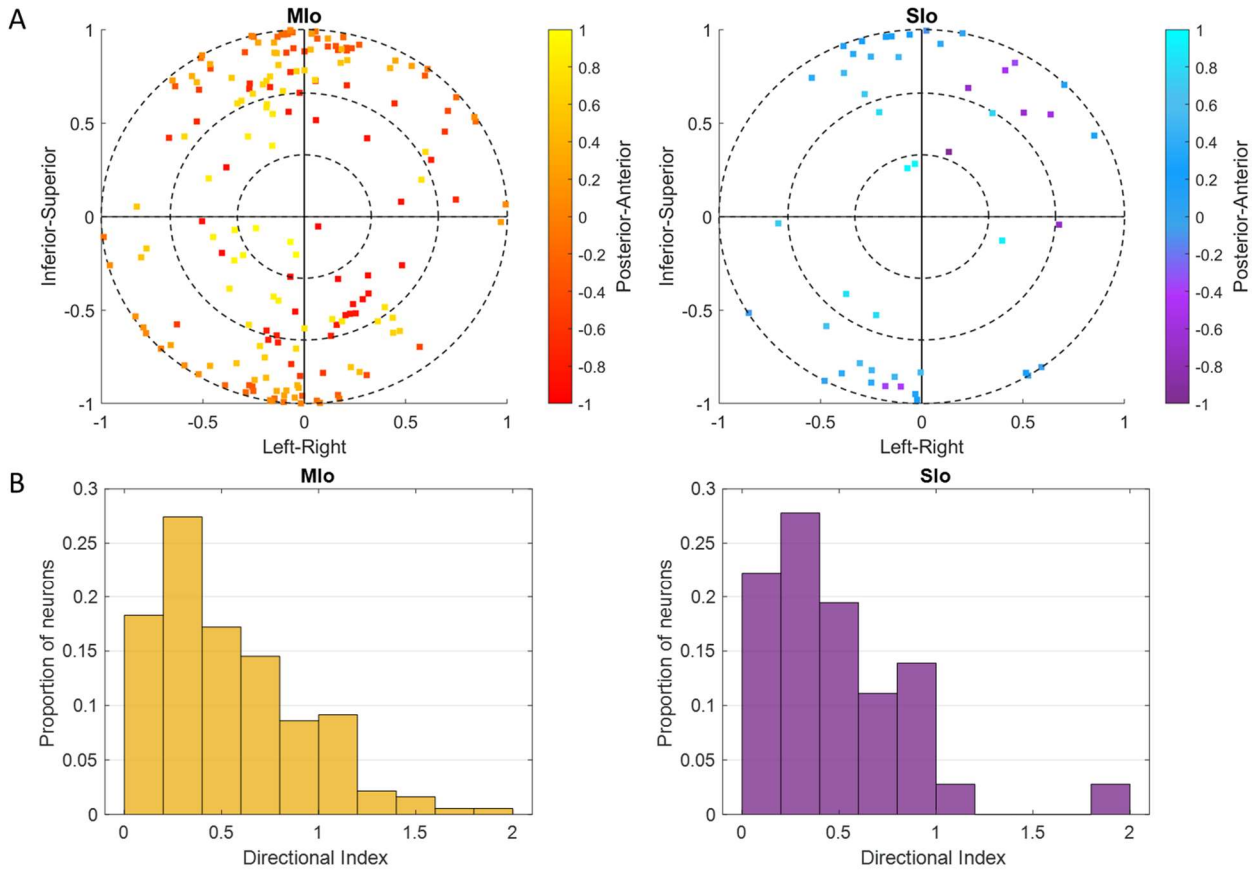

Figure 5. *Cosine tuning of MIo and SIo neurons.* ***(A)*** *Distribution of 3D preferred directions in unit sphere for neurons that fit the tuning function during feeding, combined for both subjects. The origin represents the start of a movement. Color bar represents posterior-anterior axis.* ***(B)*** *Distribution of the index for the depth of directional tuning, combined for both subjects.*

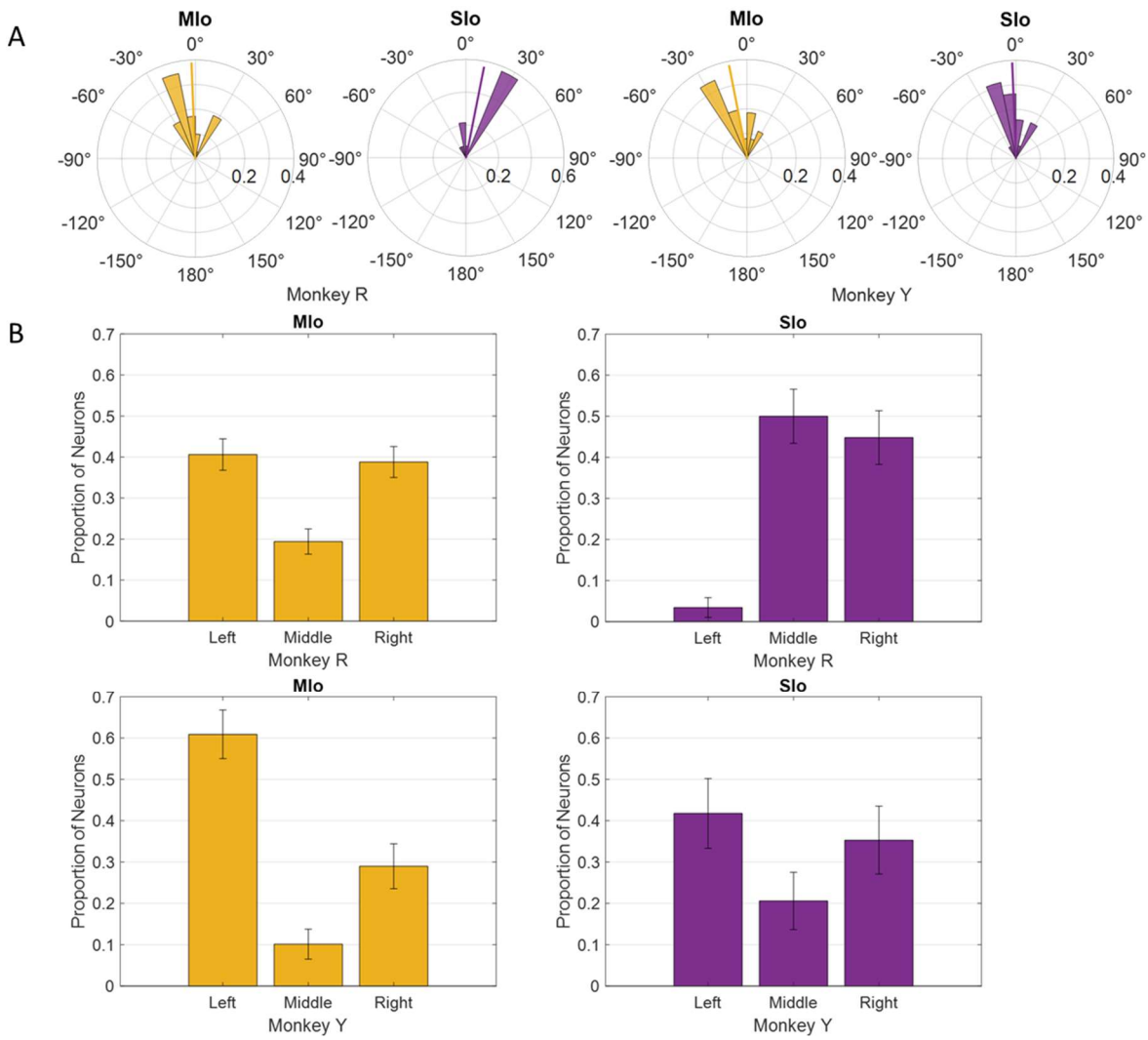

Figure 6. *Distribution of PDs in MIo (yellow) and SIo (purple) neurons during control feeding* ***(A)*** *and drinking* ***(B)****. For the feeding task, polar plots are split into 10° bins with thick colored lines representing the mean PD. For the drinking task, error bars represent ±1 SE.*

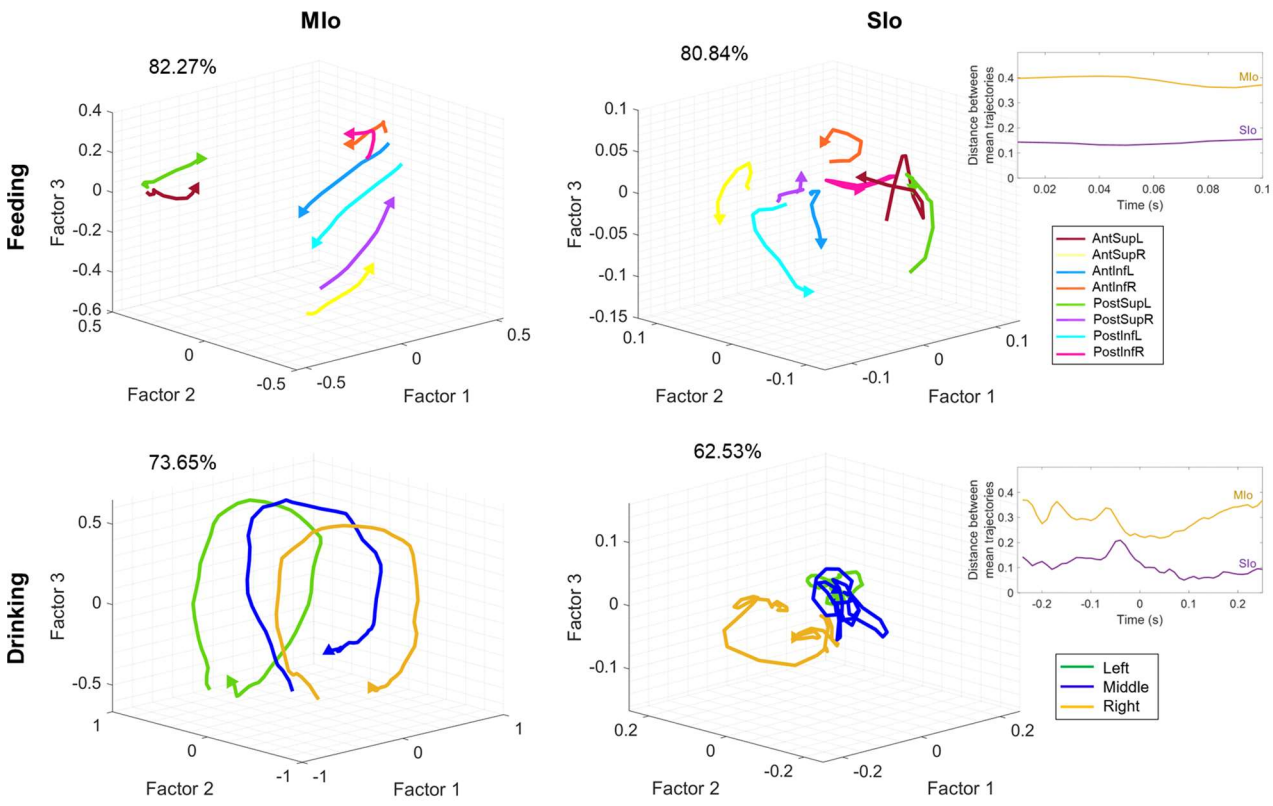

Figure 7. *Neural population trajectories vary across directions. Trial-averaged trajectories of MIo and SIo population activity along the first three latent factors for Monkey R, grouped by direction. Axes for SIo are 1/4 scale of MIo. Arrows indicate the end of the trajectory. Percentages denote the sum of the variance explained by the first three factors. Inset plots show the difference between the average inter-trajectory distances of MIo and SIo over time for both feeding and drinking.*

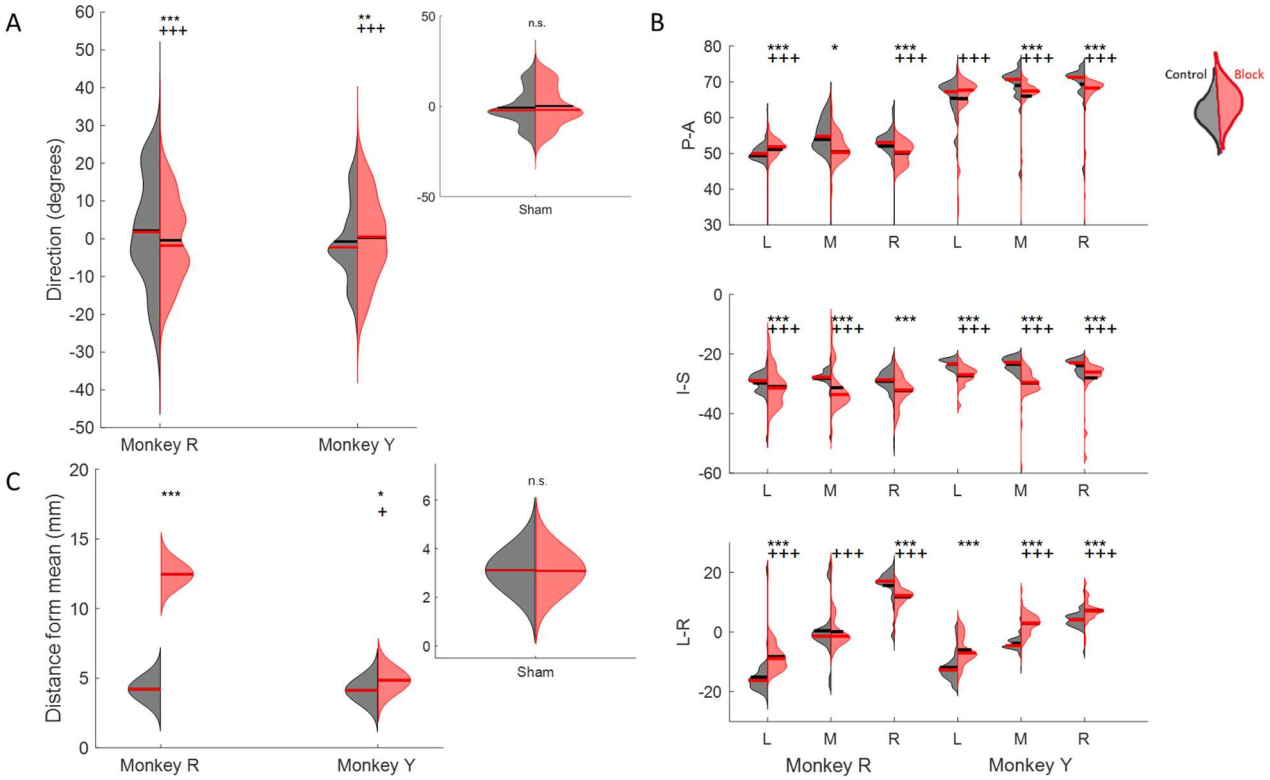

Figure 8. *Effect of nerve block on direction of tongue movement.* ***(A)*** *Distribution of tongue directions during feeding.* ***(B)*** *Variance in 3D trajectory endpoints during drinking (Posterior-Anterior, Inferior-Superior, Left-Right) for each direction: left (L), middle (M), right (R).* ***(C)*** *Variation in the distance of drinking endpoint positions from the mean endpoint. Left halves of hemi-violins (black) are control and right halves (red) are nerve block for an individual. Horizontal black lines represent the mean and horizontal red lines the median. Results of two-tailed t-test and f-test are indicated by asterisks and crosses, respectively: *,† $p < 0.05$; **,†† $p < 0.01$; ***,††† $p < 0.001$. Smaller inset plots show that there was no effect in the sham nerve block condition, for reference. The sham procedure was identical to the nerve block, except the anesthetic was substituted with saline solution*

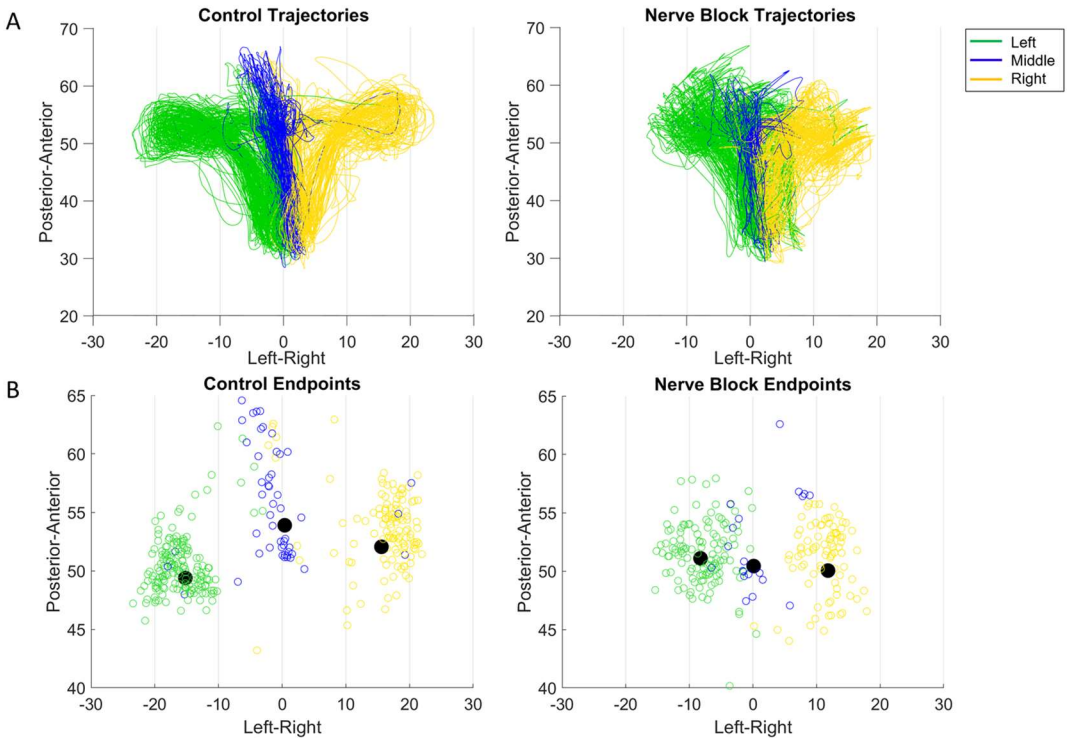

Figure 9. *Effect of nerve block on drinking kinematics in Monkey R.* ***(A)*** *Tongue tip trajectories from starting position to one of three drinking spouts in the control and nerve block conditions.* ***(B)*** *Drinking trajectory endpoints, where the black dot represents the mean endpoint position.*

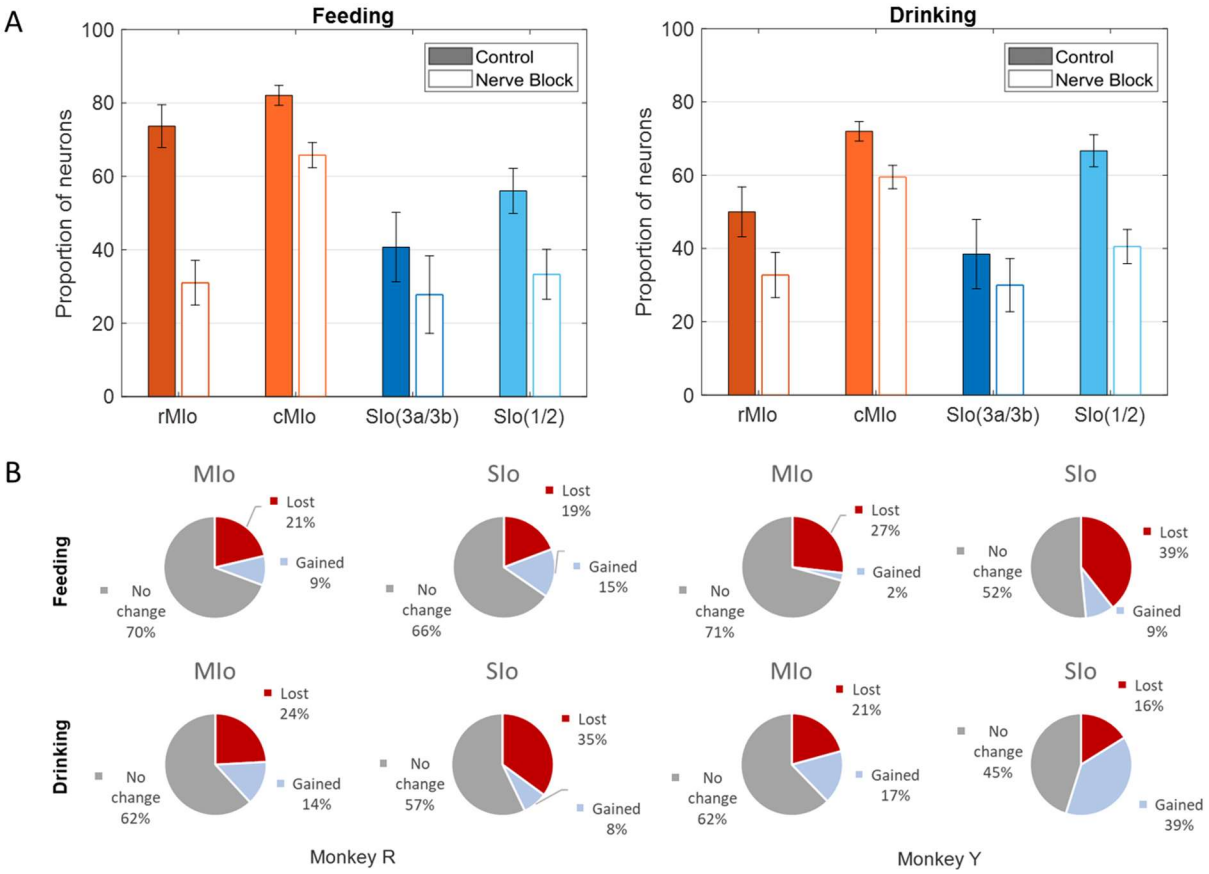

Figure 10. *Effects of nerve block on directional tuning of OSMCx neurons during feeding and drinking tasks.* ***(A)*** *Percentage of directionally tuned neurons in four areas: rMIo - rostral M1, cMIo - caudal M1, SIo(3a/3b) - area 3a/3b, and SIo(1/2) - area 1/2. Filled in bars represent control while empty bars represent nerve block. Error bars represent ±1 SE.* ***(B)*** *Percentage of MIo and SIo neurons which gained or lost directionality with the addition of nerve block.*

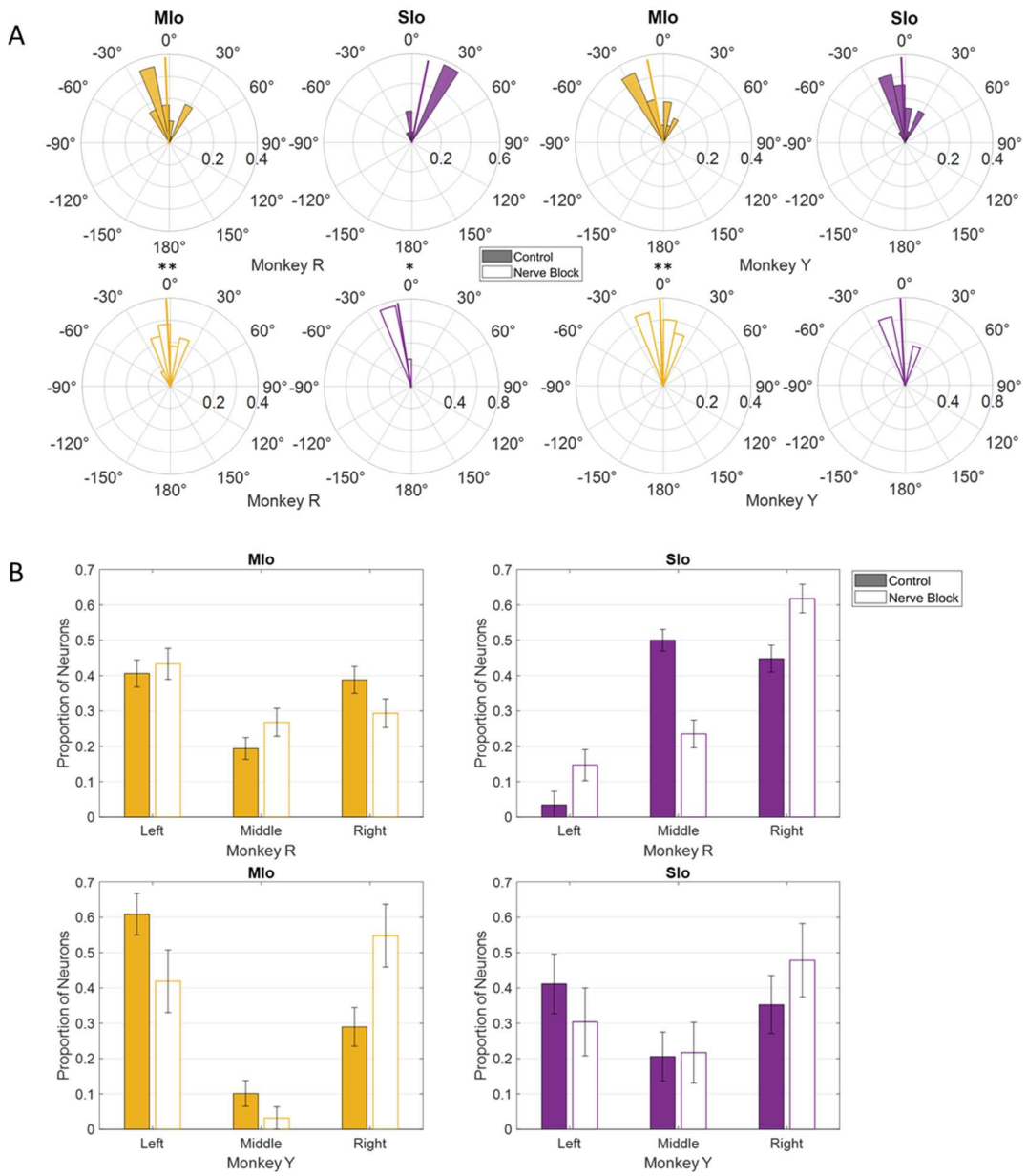

Figure 11. *Effects of nerve block on the distribution of PDs of MIo (yellow) and SIo (purple) neurons.* ***(A)*** *For the feeding task, polar plots are split into 10° bins with thick colored lines representing the mean PD. Significant circular concentration test (k-test) comparing control and nerve block are indicated by asterisks: *p < 0.05; **p < 0.01; ***p < 0.001.* ***(B)*** *For the drinking task, error bars represent ±1 SE. Filled in bars represent control while empty bars represent nerve block.*

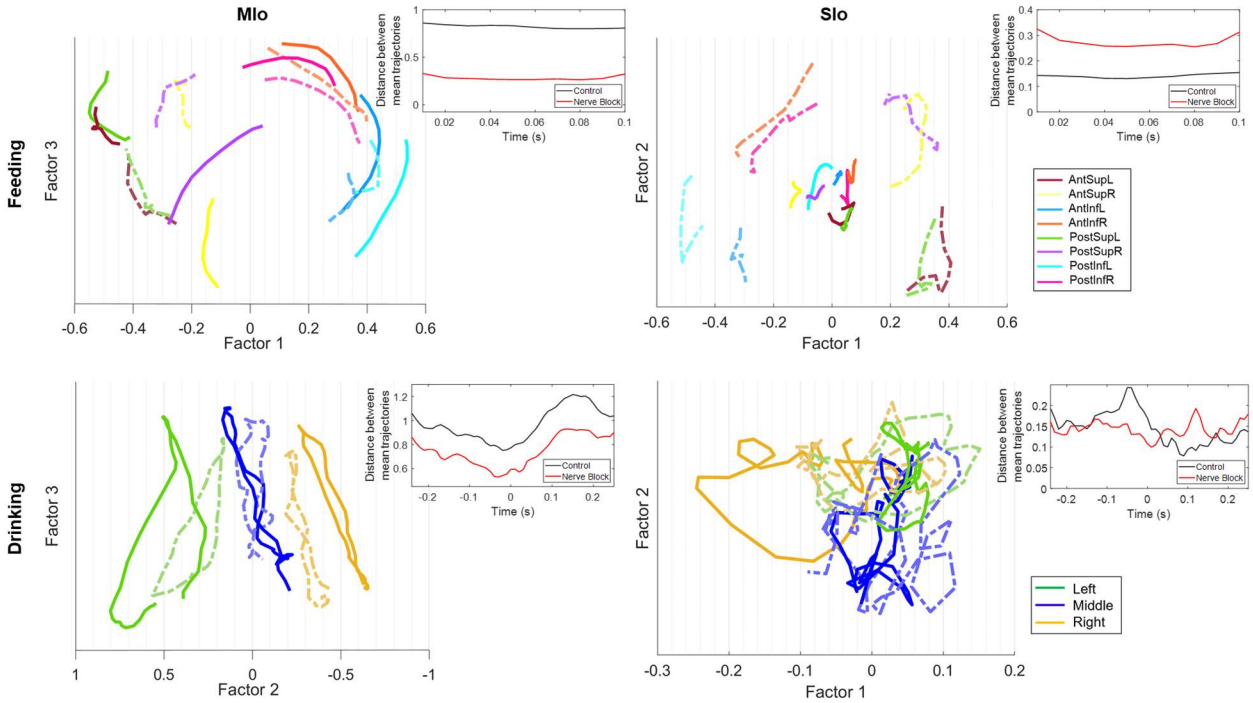

Figure 12. *Effect of nerve block on population trajectories. Trial-averaged trajectories of MIo and SIo population activity for Monkey R's feeding and drinking sessions, grouped by direction. Axes represent the latent factors from control data, with the x-axis chosen as the factor with the highest degree of separation between directions. Lighter, dotted lines represent superimposed population trajectories in the nerve block condition. Insets show the difference between the average inter-trajectory distances for control and nerve block conditions.*

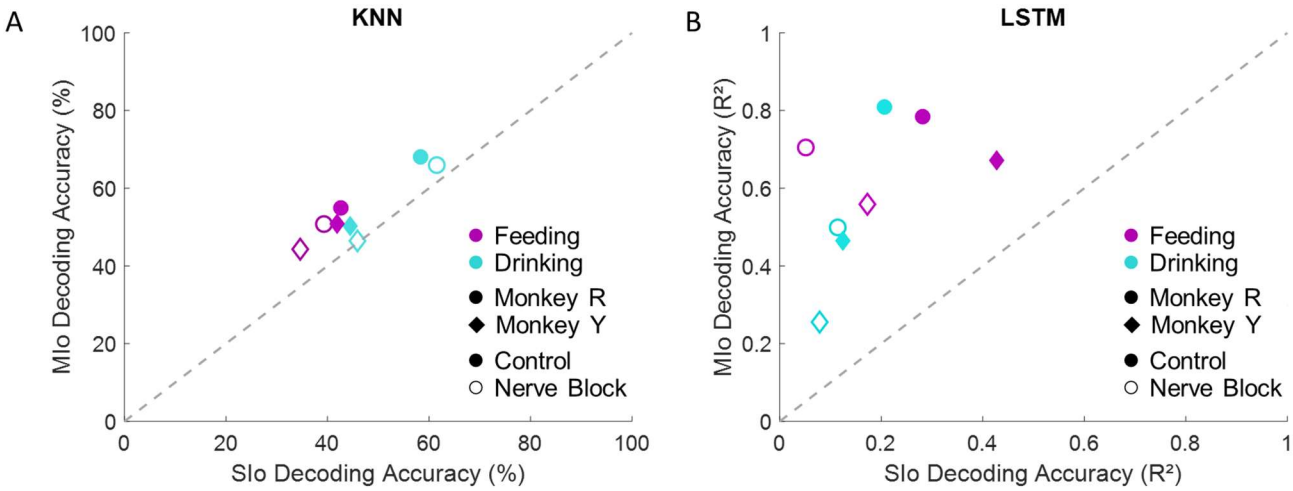

Figure 13. *Accuracies of two different decoding algorithms from MIo and SIo populations of equal size (N=28).* ***(A)*** *Comparison between average decoding accuracy of KNN classifier. Chance level is 33.33%.* ***(B)*** *Comparison between average decoding accuracy by LSTM network. Data shown separately for each subject, behavioral task, and condition. The dashed line signifies equal decoding performance for MIo and SIo. Decoding accuracies from full populations are included in Figure 13 – figure supplement 2.*